Research in Astronomy and Astrophysics

PAPER

The FAST Galactic Plane Pulsar Snapshot Survey. VIII. 116 Binary Pulsars

To cite this article: P. F. Wang *et al* 2025 *Res. Astron. Astrophys.* **25** 014003

Research in Astronomy and Astrophysics, 25:014003 (33pp), 2025 January

https://doi.org/10.1088/1674-4527/ada3b8
CSTR: 32081.14.RAA.ada3b8

The FAST Galactic Plane Pulsar Snapshot Survey. VIII. 116 Binary Pulsars

P. F. Wang[1,2,3], J. L. Han[1,2,3], Z. L. Yang[1,2], T. Wang[1], C. Wang[1,2,3], W. Q. Su[1,2], J. Xu[1,3], D. J. Zhou[1], Yi Yan[1], W. C. Jing[1,2], N. N. Cai[1], J. P. Yuan[4], R. X. Xu[5,6], H. G. Wang[7], and X. P. You[8]
[1] National Astronomical Observatories, Chinese Academy of Sciences, Beijing 100101, China; pfwang@nao.cas.cn, hjl@nao.cas.cn
[2] School of Astronomy and Space Science, University of Chinese Academy of Sciences, Beijing 100049, China
[3] Key Laboratory of Radio Astronomy and Technology, Chinese Academy of Sciences, Beijing 100101, China
[4] Xinjiang Astronomical Observatory, Chinese Academy of Sciences, Urumqi 830011, China
[5] Department of Astronomy, Peking University, Beijing 100871, China
[6] Kavli Institute for Astronomy and Astrophysics, Peking University, Beijing 100871, China
[7] Department of Astronomy, School of Physics and Materials Science, Guangzhou University, Guangzhou 510006, China
[8] School of Physical Science and Technology, Southwest University, Chongqing 400715, China
Received 2024 October 22; revised 2024 December 4; accepted 2024 December 10; published 2025 January 31

Abstract

Finding pulsars in binaries is important for measurements of the masses of neutron stars (NSs), for tests of gravity theories, and for studies of star evolution. We are carrying out the Galactic Plane Pulsar Snapshot survey (GPPS) by using the Five-hundred-meter Aperture Spherical radio Telescope (FAST). Here we present the Keplerian parameters for 116 newly discovered pulsars in the FAST GPPS survey and obtain timing solutions for 29 pulsars. Companions of these pulsars are He white dwarfs (WDs), CO/ONe WDs, NSs, main sequence stars and ultra light objects or even planets. Our observations uncover eclipses of eight binary systems. The optical counterpart for the companion of PSR J1908+1036 is identified. The Post-Keplerian parameter $\dot{\omega}$ for the double NS systems PSR J0528+3529 and J1844-0128 have been measured, with which the total masses of the binary systems are determined.

Key words: (stars:) pulsars: general – (stars:) binaries: general – stars: neutron

1. Introduction

Pulsars are rapidly rotating neutron stars (NSs) with spin periods ranging from about 1.39 milliseconds to several tens of seconds (Manchester et al. 2005, see updated catalog 2.4.0[9]). They are formed through supernova explosion of massive stars (8–25$M_\odot$) at the end of stellar evolution or accretion-induced collapse of massive white dwarfs (WDs). Pulsars serve as important laboratories for studying fundamental physics due to their super high density, extremely strong magnetic field and gravitational field. They have been employed to detect low-frequency gravitational waves through pulsar timing arrays (e.g., Lentati et al. 2015; Alam et al. 2021; Reardon et al. 2021; Xu et al. 2023), test the theory of gravity (e.g., Freire et al. 2012), constrain the equation of state (EOS) of NS by mass measurement (e.g., Demorest et al. 2010; Antoniadis et al. 2013; Özel & Freire 2016), and construct pulsar-based timescale (Hobbs et al. 2020).

Among 3724 known pulsars (Manchester et al. 2005), 421 pulsars are in binary systems. Most of the pulsars in binary systems are millisecond pulsars (MSPs) with spin periods of $P \leqslant 30$ ms and spin-down rate $\dot{P} \leqslant 10^{-17}$. These binary MSPs are generally believed to be spun up by accreting material from their companion (e.g., Alpar et al. 1982; Bhattacharya & van den Heuvel 1991), so they are called "recycled pulsars." During recycling, the magnetic field strength of pulsars is reduced and their orbits are circularized. Companions of these binary pulsars can be NSs, WDs, main sequence stars (MS), ultra-light companions (UL) such as brown dwarf or WD remnants or planets with mass $m_c \leqslant 0.1 M_\odot$. The spin periods P, pulsar ellipses, orbital periods P_b, orbital eccentricity e and median companion masses $m_{c,med}$ derived from mass functions can be used as criteria to classify companion types, see Table 1. For example, some MSPs in compact orbits ($P_b < 1$ day) with a low-mass non- or semi-degenerate companion are "spiders," in which the pulsar winds are evaporating the companion. Many of them show the eclipses of pulsar signals. They are further divided into "black-widows" if the companion mass is less than ~$0.1 M_\odot$, or "redbacks" if the companion mass is greater than ~$0.1 M_\odot$ and such companions have probably evolved MSs (Chen et al. 2013; Roberts 2013).

Binary systems have diverse formation histories. It is generally accepted that double NS systems originate from high-mass X-ray binaries (HMXBs) via a common envelope (CE) and spiral-in process (e.g., Tauris & van den Heuvel 2006). Pulsars with CO/ONe-WD companions originate from intermediate-mass X-ray binaries (IMXBs, e.g., Tauris et al. 2012), and the ones with He-WD companions originate from low-mass X-ray binaries (LMXBs, e.g., Pylyser & Savonije 1988; Istrate et al. 2014). The final orbital

[9] www.atnf.csiro.au/people/pulsar/psrcat/

Table 1
Parameter Ranges for Known Binary Pulsars with Various Companion Types in the Galactic Field and the Classification Criteria

Companion Type	P (ms)	P_b (days)	$m_{c,med}$ ($M_\odot$)	e	Coarse Classification Criteria
He-WD	[1.74, 834.84]	[0.10, 944.64]	[0.07, 0.48]	[1.2×10^{-7}, 0.14]	$m_{c,med} > 0.08M_\odot$ and $P < 10$ ms and [($m_{c,med} < 0.356M_\odot$ and $P_b < 100$ days) or ($m_{c,med} < 0.5M_\odot$ and $P_b > 100$ days)]
CO/ONe-WD	[2.91, 1066.37]	[0.19, 95.26[a]]	[0.33[a], 1.58]	[6.9×10^{-7}, 0.66]	$m_{c,med} > 0.356M_\odot$ and $P_b < 100$ days and $e < 0.05$
Ultra-light object (UL)	[1.41, 520.95]	[0.06, 10.59]	[0.0009, 0.097]	[2.6×10^{-6}, 4.5×10^{-3}]	$m_{c,med} < 0.08M_\odot$
MS star (unevolved)	[47.76[b], 763.93]	[95.17, 16800]	[1.08, 18.50]	[0.08, 0.96]	$m_{c,med} > 1.0M_\odot$ and $P_b > 80$ days and $e > 0.05$ and $P > 30$ ms
MS star (evolved)	[1.61, 14.25]	[0.08, 1.1[c]]	[0.11, 0.52]	[4.2×10^{-6}, 2.1×10^{-4}]	$0.1M_\odot < m_{c,med} < 0.52M_\odot$ and $P_b < 1.1$ days and $e < 0.001$ and $P < 30$ ms and Eclipse
Neutron star (NS)	[16.96 2773.46]	[0.078, 45.06]	[0.76, 1.74]	[0.06, 0.83]	$m_{c,med} > 0.76M_\odot$ and $P_b < 80$ days and $e > 0.05$

Notes. The above parameter spaces are rough indicators for the classification of binary types. However, there have been some exceptions. For example.
[a] J0823+0159 has a CO-WD companion with an orbital period of 1232.4 days and a median mass of $0.226M_\odot$ (Koester & Reimers 2000).
[b] J1903+0327 has an MS companion, a spin period of 2.150 ms and an orbital period of 95.2 days (Freire et al. 2011).
[c] J1417–4402 has a red-giant companion with an orbital period of 5.4 days (Strader et al. 2015).

Table 2
FAST Projects for Collecting Data for Binary Pulsar Timing in this Paper

Project ID	PI	Observation Hours
ZD2020_2	J. L. Han	350+
ZD2021_2	J. L. Han	350+
ZD2022_2	J. L. Han	350+
ZD2023_2	J. L. Han	350+
ZD2024_2	J. L. Han	350+
PT2020_0136	P. F. Wang	30.0
PT2021_0037	T. Wang	42.0
PT2021_0126	P. F. Wang	40.0
PT2022_0047	W. Q. Su	70.0
PT2022_0158	Z. L. Yang	20.0
PT2022_0159	T. Wang	20.0
PT2022_0174	P. F. Wang	20.0
PT2022_0178	Z. L. Yang	15.0
PT2023_0084	Z. L. Yang	18.9
PT2023_0085	P. F. Wang	19.5
PT2023_0143	Z. L. Yang	15.8
PT2023_0162	W. Q. Su	11.5
PT2023_0190	P. F. Wang	7.6
PT2023_0193	Z. L. Yang	11.5
PT2023_0195	Z. L. Yang	11.2
PT2024_0007	P. F. Wang	23.3
PT2024_0020	Z. L. Yang	31.9
PT2024_0026	P. F. Wang	25.0
PT2024_0200	Z. L. Yang	13.1
PT2024_0224	W. C. Jing	5.6
PT2024_0231	Z. L. Yang	5.4

configuration and stellar masses are diverse, depending on the companion mass and metallicity, the initial orbital separation as well as the evolution stage of the donor star when Roche-Lobe Overflow (RLO) initiates, for example, the Case A RLO on the main sequence stage, the Case B RLO at the red-giant branch stage with hydrogen shell burning, the Case C RLO for the asymptotic giant branch stage with helium shell burning (e.g., Tauris & van den Heuvel 2023). Hence, the spin period, period derivative, orbital period, orbit eccentricity, and masses of the pulsar and its companion are important fossil records for the original binary evolution (e.g., Corbet 1984; Phinney 1992). Based on observations of binary pulsars, the evolution theories of stellar binaries have been developed and examined (e.g., Tauris et al. 2012; Istrate et al. 2014; Chen et al. 2021).

Binary systems with compact orbits generally exhibit a number of relativistic effects which can be quantified by Post-Keplerian (PK) parameters. With two PK parameters, the masses of the pulsar and the companion as well as the inclination angle of the orbit can be determined by resorting to a theory of gravity, e.g., General Relativity (GR) (e.g., Özel & Freire 2016). By combining these precisely measured pulsar masses, the underlying distribution of NS masses can be determined (Antoniadis et al. 2016). Masses of the most massive NSs pose important constraints on the EOS of NSs, e.g., PSRs J0348+0432, J0740+6620 and J1614–2230 (e.g., Demorest et al. 2010; Antoniadis et al. 2013; Özel & Freire 2016). So the measured companion masses can be employed to test the theories of binary evolution (Phinney & Kulkarni 1994; Tauris & Savonije 1999). The combination of more than two PK parameters allows for the tests of GR and other theories of gravity in the strong-field regime with high precision (Weisberg & Taylor 1984; Kramer et al. 2006). The violation of the strong equivalence principle can also be tested by constraining the universality of freefall or gravitational dipole radiation (Freire et al. 2012; Voisin et al. 2020).

Table 3
Binary Parameters of 116 GPPS Pulsars

Pulsar Name	R.A. (h:m:s)	Decl. (d:m:s)	DM (cm^{-3} pc)	P (ms)	P_b (days)	x (lt-s)	e	f ($M_\odot$)	$m_{c,min}$ ($M_\odot$)	$m_{c,med}$ ($M_\odot$)	Comp.	Ref. and notes
(1)	(2)	(3)	(4)	(5)	(6)	(7)	(8)	(9)	(10)	(11)	(12)	(13)
J0416+5201 (gpps0560)	04:16:27.277	+52:01:25.76	140.49	18.240556	0.396469	3.50556	4.6×10^{-5}	0.2943	1.261	1.568	CO/ONe	(1)
J0520+3722 (gpps0538)	05:20:13.564	+37:22:09.53	88.98	7.913261	0.579675	3.37242	1.0×10^{-6}	0.1226	0.837	1.019	CO/ONe	(1)
J0528+3529 (gpps0537)	05:28:28.798	+35:29:36.87	111.83	78.233675	11.726180	31.43462	0.290	0.2425	1.148	1.420	NS	(0)
J0622+0339 (gpps0388)	06:22:19.486	+03:39:42.88	79.41	8.771533	9.546266	4.89181	1.1×10^{-5}	1.379×10^{-3}	0.146	0.170	He	(0)
J1838+0024 (gpps0107)	18:38:23.385	+00:24:20.65	122.63	5.087126	8.415011	2.64365	4.2×10^{-5}	2.801×10^{-4}	0.083	0.097	He	(0)
J1840+0012 (gpps0146)	18:40:49.206	+00:12:30.00	100.84	5.338973	0.328567	0.52890	3.5×10^{-5}	1.471×10^{-3}	0.149	0.174	He	(0)
J1844–0128 (gpps0555)	18:44:20.995	–01:28:25.77	368.18	29.144422	10.600318	20.96778	0.235	8.809×10^{-2}	0.724	0.876	NS	(0)
J1844+0028 (gpps0109)	18:44:37.359	+00:28:12.58	181.09	3.570671	1.078895	1.05955	4.9×10^{-5}	1.097×10^{-3}	0.134	0.156	He	(0)
J1845+0201 (gpps0547)	18:45:03.077	+02:01:49.36	56.65	4.309250	5.325708	4.55180	1.7×10^{-5}	3.570×10^{-3}	0.205	0.240	He	(0)
J1845+0317 (gpps0566)	18:45:22.886	+03:17:18.59	77.26	1.850702	0.190099	0.01514	3.7×10^{-3}	1.032×10^{-7}	0.006	0.007	UL	(0)
J1857+0642 (gpps0236)	18:57:58.678	+06:42:30.65	21.58	3.530989	6.734521	8.78290	6.6×10^{-6}	1.604×10^{-2}	0.361	0.427	CO/He	(0)
J1901+0658 (gpps0001)	19:01:22.851	+06:58:24.13	125.88	75.743850	14.454772	32.40203	0.366	0.1748	0.984	1.207	NS	(2)
J1903+0839 (gpps0100)	19:03:51.845	+08:39:17.19	166.45	4.621169	0.312639	0.40500	5.6×10^{-6}	7.297×10^{-4}	0.116	0.135	He	(0)
J1904+0553 (gpps0039)	19:04:16.822	+05:53:53.61	164.27	4.907323	1.583625	1.41774	6.7×10^{-6}	1.220×10^{-3}	0.139	0.163	He	(0)
J1905+0649 (gpps0229)	19:05:05.257	+06:49:49.33	187.66	27.464412	1.381714	6.62159	2.5×10^{-5}	0.1633	0.953	1.168	CO/ONe	(0)
J1908+1036 (gpps0114)	19:08:21.521	+10:36:35.36	10.91	10.690195	3.964125	11.38825	6.9×10^{-7}	0.1009	0.768	0.932	CO/ONe	(0)
J1911+1253 (gpps0181)	19:11:28.699	+12:53:17.41	68.68	27.238703	11.789053	20.43727	0.005	6.595×10^{-2}	0.639	0.770	CO/ONe	(0)
J1912+1416 (gpps0169)	19:12:30.513	+14:16:23.67	66.66	3.166241	0.246894	0.32981	1.1×10^{-5}	6.319×10^{-4}	0.110	0.129	He	(0)
J1916+0740 (gpps0166)	19:16:15.432	+07:40:41.17	219.86	11.219660	14.818414	7.31559	2.1×10^{-5}	1.914×10^{-3}	0.164	0.191	He	(0)
J1917+0615 (gpps0460)	19:17:20.288	+06:15:29.19	172.47	3.967699	4.618437	3.55159	4.6×10^{-5}	2.255×10^{-3}	0.174	0.203	He	(0)
J1917+1259 (gpps0012)	19:17:21.337	+12:59:59.82	117.01	5.637468	3.201264	5.89628	4.8×10^{-5}	2.148×10^{-2}	0.404	0.480	CO/He	(0)
J1918+0621 (gpps0494)	19:18:00.606	+06:21:59.38	63.11	2.103682	4.449196	2.73700	4.2×10^{-5}	1.112×10^{-3}	0.135	0.157	He	(0)
J1919+1341 (gpps0215)	19:19:23.012	+13:41:09.28	394.56	11.655722	0.370338	2.34094	1.0×10^{-5}	0.1004	0.766	0.930	CO/ONe	(1)
J1924+1342 (gpps0032)	19:24:16.597	+13:42:50.07	98.34	5.721085	3.528174	1.60733	4.8×10^{-5}	3.582×10^{-4}	0.091	0.105	He	(0)
J1928+1815 (gpps0121)	19:28:08.349	+18:15:30.26	346.14	10.549499	0.149902	1.69862	8.6×10^{-6}	0.2342	1.129	1.395	He MS	(3), Eclipse
J1930+1403 (gpps0013)	19:30:17.620	+14:03:53.80	150.48	3.209448	5.574928	5.18040	1.9×10^{-5}	4.803×10^{-3}	0.229	0.269	He	(0)
J1932+2121 (gpps0403)	19:32:21.201	+21:21:06.78	192.10	14.244703	0.080905	0.16269	2.8×10^{-5}	7.063×10^{-4}	0.115	0.134	MS	(0), Eclipse
J1936+2035 (gpps0197)	19:36:38.307	+20:35:47.29	198.86	32.927683	1.064143	5.64685	5.3×10^{-5}	0.1707	0.973	1.193	CO/ONe	(0)
J1938+2302 (gpps0392)	19:38:11.630	+23:02:00.16	303.36	52.761755	33.969877	54.67080	4.0×10^{-4}	0.1520	0.922	1.129	CO/ONe	(0)
J1943+2206 (gpps0514)	19:43:43.648	+22:06:33.26	211.10	4.681671	26.762465	23.79641	3.3×10^{-5}	2.020×10^{-2}	0.395	0.468	CO/He	(0)
J1943+2210 (gpps0227)	19:43:53.777	+22:10:33.97	110.66	12.870079	0.372052	2.57981	1.7×10^{-6}	0.1332	0.869	1.060	CO/ONe	(1)
J1946+0904 (gpps0242)	19:46:56.870	+09:04:53.33	37.18	25.772259	6.037962	7.13524	3.4×10^{-4}	1.070×10^{-2}	0.309	0.364	CO/He	(0)
J1947+2011 (gpps0011)	19:47:47.713	+20:11:00.45	127.49	8.177551	81.968910	37.80393	1.4×10^{-4}	8.634×10^{-3}	0.285	0.335	He	(0)
J1947+2304 (gpps0379)	19:47:28.937	+23:04:15.30	320.99	10.893691	0.338881	2.39708	1.6×10^{-5}	0.1288	0.856	1.043	CO/ONe	(1)
J1952+2837 (gpps0064)	19:52:49.653	+28:37:12.91	313.17	18.020942	0.867494	1.66242	8.1×10^{-6}	6.555×10^{-3}	0.257	0.302	CO/He	(0)
J1953+1844 (gpps0190)	19:53:37.946	+18:44:54.31	113.11	4.444080	0.037039	0.00666	5.5×10^{-4}	2.312×10^{-7}	0.0075	0.0087	UL	(4)
J2018+3518 (gpps0393)	20:18:48.149	+35:18:45.85	266.99	31.316219	3.332715	12.44297	4.3×10^{-5}	0.1862	1.013	1.245	CO/ONe	(0)
J2023+2853 (gpps0201)	20:23:21.063	+28:53:41.45	22.75	11.328905	0.718230	4.00222	1.3×10^{-5}	0.1334	0.869	1.061	CO/ONe	(1)
J0408+4955g (gpps0638)	04:08:07	+49:55	73.7	11.44457	2.9910	9.9122	⋯	0.1169	0.819	0.997	CO/ONe	
J0541+2959g (gpps0535)	05:41:44	+29:59	67.3	3.20648	0.3754	0.2289	⋯	9.138×10^{-5}	0.057	0.066	UL	
J1814+0045g (gpps0549)	18:14:10	+00:45	124.0	2.30854	0.2023	0.1477	⋯	8.453×10^{-5}	0.055	0.064	UL	Eclipse
J1819–0050g (gpps0581)	18:19:30	–00:50	103.3	6.60125	8.8132	17.6135	⋯	7.554×10^{-2}	0.677	0.817	CO/ONe	
J1821+0007g (gpps0613)	18:21:02	+00:07	55.2	4.22205	8.0000	5.5350	⋯	2.845×10^{-3}	0.189	0.221	He	
J1821+0044g (gpps0591)	18:21:31	+00:44	126.8	2.71314	2.3158	1.7697	⋯	1.110×10^{-3}	0.135	0.157	He	
J1829–0235g (gpps0599)	18:29:35	–02:35	103.3	7.42749	0.9680	1.0035	⋯	1.158×10^{-3}	0.137	0.160	He	
J1830–0106g (gpps0409)	18:30:07	–01:06	149.4	1.75841	0.1066	0.0810	⋯	5.021×10^{-5}	0.046	0.053	UL	
J1833–0046g (gpps0365)	18:33:53	–00:46	81.4	2.95373	55.3724	13.7231	⋯	9.050×10^{-4}	0.125	0.146	He	

Table 3
(Continued)

Pulsar Name (1)	R.A. (h:m:s) (2)	Decl. (d:m:s) (3)	DM (cm^{-3} pc) (4)	P (ms) (5)	P_b (days) (6)	x (lt-s) (7)	e (8)	f ($M_\odot$) (9)	$m_{c,min}$ ($M_\odot$) (10)	$m_{c,med}$ ($M_\odot$) (11)	Comp. (12)	Ref. and notes (13)
J1835–0011g (gpps0221)	18:35:46	–00:11	36.2	3.22936	7.1903	5.8878	···	4.239×10^{-3}	0.218	0.256	He	
J1835+0158g (gpps0636)	18:35:22	+01:58	181.5	3.31989	12.7241	9.1303	···	5.048×10^{-3}	0.233	0.274	He	
J1836–0150g (gpps0394)	18:36:05	–01:50	199.5	5.45772	51.4903	21.5515	···	4.054×10^{-3}	0.215	0.252	He	
J1836+0117g (gpps0592)	18:36:11	+01:17	178.0	3.81164	24.1087	5.7377	···	3.489×10^{-4}	0.090	0.104	He	
J1837+0528g (gpps0204)	18:37:40	+05:28	120.8	6.25958	21.7247	16.4399	···	1.011×10^{-2}	0.302	0.356	He	
J1838–0156g (gpps0267)	18:38:06	–01:56	163.4	5.50730	6.6937	5.7062	···	4.452×10^{-3}	0.222	0.261	He	
J1838+0028g (gpps0350)	18:38:31	+00:28	107.3	1.86540	7.5914	8.9852	···	1.352×10^{-2}	0.338	0.399	CO/He	
J1838+1507g (gpps0245)	18:38:36	+15:07	54.7	3.81818	0.1119	0.0512	···	1.151×10^{-5}	0.028	0.032	UL	
J1839+0100g (gpps0419)	18:39:27	+01:00	130.1	5.36859	87.6694	32.1057	···	4.623×10^{-3}	0.226	0.265	He	
J1842–0138g (gpps0565)	18:42:31	–01:38	209.9	2.70823	1.0943	1.0044	···	9.061×10^{-4}	0.125	0.146	He	
J1842+0407g (gpps0417)	18:42:11	+04:07	101.6	3.93875	4.3777	5.9280	···	1.167×10^{-2}	0.319	0.377	He/CO/ONe	
J1845+0104g (gpps0224)	18:45:50	+01:04	95.0	6.71362	3.8658	3.7613	···	3.823×10^{-3}	0.210	0.247	He	
J1846+0507g (gpps0614)	18:46:50	+05:07	101.6	3.07255	19.4795	11.2908	···	4.073×10^{-3}	0.215	0.252	He	
J1847+0342g (gpps0431)	18:47:30	+03:42	81.1	4.28904	0.1392	0.0360	···	2.585×10^{-6}	0.017	0.020	UL	
J1849+0304g (gpps0342)	18:49:32	+03:04	146.7	1.79342	0.2412	0.7614	···	8.146×10^{-3}	0.278	0.328	MS	Eclipse
J1849+0623g (gpps0485)	18:49:50	+06:23	129.2	14.58764	6.9840	11.6331	···	3.465×10^{-2}	0.489	0.584	CO/ONe	
J1852+0309g (gpps0171)	18:52:10	+03:09	358.0	5.57683	12.9014	16.5022	···	2.899×10^{-2}	0.455	0.543	CO/ONe	
J1853–0008Ag (gpps0193)	18:53:12	–00:08	285.2	2.82485	77.9991	28.3801	···	4.034×10^{-3}	0.215	0.252	He	
J1854+0012g (gpps0020)	18:54:16	+00:13	204.1	2.70923	7.4103	5.5362	···	3.318×10^{-3}	0.200	0.234	He	
J1856+1000g (gpps0331)	18:56:30	+10:00	202.1	4.86584	10.5916	2.2154	···	1.041×10^{-4}	0.059	0.069	UL	
J1857–0125g (gpps0396)	18:57:21	–01:25	213.9	1.83371	0.2385	0.5575	···	3.271×10^{-3}	0.199	0.233	He/MS	
J1857–0230g (gpps0577)	18:57:20	–02:30	134.5	35.15683	29.4902	53.7076	···	0.1913	1.026	1.262	CO/ONe	
J1858–0128g (gpps0425)	18:58:11	–01:28	38.1	7.87566	96.9722	42.0315	···	8.487×10^{-3}	0.283	0.333	He	
J1858+0244g (gpps0125)	18:58:01	+02:44	282.7	2.61247	91.6645	25.8920	···	2.218×10^{-3}	0.173	0.202	He	
J1859+0026Ag (gpps0066)	18:59:58	+00:26	334.1	8.57234	95.1021	40.3135	···	7.778×10^{-3}	0.274	0.322	He	
J1859+0313g (gpps0131)	18:59:35	+03:13	107.8	1.61335	0.4443	1.1770	···	8.869×10^{-3}	0.288	0.339	MS	Eclipse
J1859+0658g (gpps0162)	18:59:04	+06:58	290.4	5.11175	9.2967	6.9825	···	4.229×10^{-3}	0.218	0.256	He	
J1900+0213g (gpps0063)	19:00:12	+02:13	309.9	32.09151	826.6043	309.3251	···	4.651×10^{-2}	0.552	0.662	CO/He	
J1902+0011g (gpps0442)	19:02:40	+00:11	248.5	5.92786	42.2831	20.8540	···	5.446×10^{-3}	0.240	0.282	He	
J1903+0830g (gpps0531)	19:03:39	+08:30	334.8	4.08534	6.0782	4.4347	···	2.535×10^{-3}	0.181	0.212	He	
J1904+0056g (gpps0441)	19:04:58	+00:56	51.4	5.85050	19.1627	22.6699	···	3.407×10^{-2}	0.486	0.580	CO/ONe	
J1904+0836g (gpps0104)	19:04:35	+08:36	90.5	4.43642	6.0242	4.9921	···	3.681×10^{-3}	0.207	0.243	He	
J1907+0009g (gpps0588)	19:07:21	+00:09	83.0	2.37558	6.1895	5.0710	···	3.655×10^{-3}	0.207	0.243	He	
J1907+0014g (gpps0579)	19:07:56	+00:14	172.6	24.51782	4.0846	15.5954	···	0.2441	1.152	1.425	CO/ONe	
J1907+0052g (gpps0600)	19:07:57	+00:52	162.9	2.92067	6.1830	3.1321	···	8.630×10^{-4}	0.123	0.114	He	
J1908+0029g (gpps0633)	19:08:30	+00:29	165.3	3.41581	2.0753	2.0276	···	2.078×10^{-3}	0.169	0.197	He	
J1908+0705g (gpps0278)	19:08:55	+07:04	41.4	1.99057	0.8509	0.9260	···	1.177×10^{-3}	0.138	0.161	He	
J1908+0949g (gpps0128)	19:08:07	+09:49	220.1	9.04837	2.8725	3.8534	···	7.446×10^{-3}	0.269	0.317	He/CO	
J1910+0423g (gpps0432)	19:10:10	+04:23	339.9	93.24143	893.6631	222.6467	···	1.484×10^{-2}	0.350	0.414	He/CO	
J1910+1054g (gpps0049)	19:10:01	+10:54	139.3	3.87080	65.4001	28.4605	···	5.787×10^{-3}	0.245	0.288	He	
J1911+1206g (gpps0235)	19:11:24	+12:06	181.7	3.44012	0.1724	0.0150	···	1.294×10^{-7}	0.006	0.007	UL	
J1915+0720g (gpps0413)	19:15:35	+07:20	122.1	5.69055	4.5372	3.3045	···	1.882×10^{-3}	0.163	0.190	He	
J1917+1046g (gpps0157)	19:17:55	+10:46	163.1	87.73271	827.99	236.13	···	2.062×10^{-2}	0.398	0.472	He/CO	
J1918+1536g (gpps0145)	19:18:23	+15:36	123.4	109.93966	20.5750	31.5020	···	7.929×10^{-2}	0.691	0.835	CO/ONe	
J1918+1540g (gpps0144)	19:18:19	+15:40	271.1	4.28381	14.8603	19.7143	···	3.725×10^{-2}	0.504	0.602	CO/ONe	
J1918+1546 (gpps0160)	19:18:35.613	+15:46:51.59	64.64	3.764172	4.673381	4.02845	···	3.217×10^{-3}	0.197	0.231	He	
J1919+0126g (gpps0383)	19:19:23	+01:26	125.2	1.89736	0.2694	0.0806	···	7.746×10^{-6}	0.024	0.028	UL	
J1919+1502g (gpps0411)	19:19:57	+15:02	232.8	3.64606	0.1119	0.1686	···	4.110×10^{-4}	0.095	0.110	MS	Eclipse

Table 3
(Continued)

Pulsar Name (1)	R.A. (h:m:s) (2)	Decl. (d:m:s) (3)	DM (cm^{-3} pc) (4)	P (ms) (5)	P_b (days) (6)	x (lt-s) (7)	e (8)	f ($M_{\odot}$) (9)	$m_{c,min}$ ($M_{\odot}$) (10)	$m_{c,med}$ ($M_{\odot}$) (11)	Comp. (12)	Ref. and notes (13)
J1921+1216g (gpps0237)	19:21:03	+12:16	256.2	3.00144	8.4166	6.0642	⋯	3.380×10^{-3}	0.201	0.236	He	
J1921+1652g (gpps0336)	19:21:34	+16:52	124.1	3.68199	2.7022	1.6514	⋯	6.622×10^{-4}	0.112	0.131	He	
J1923+2022g (gpps0155)	19:23:46	+20:22	175.3	37.99289	776.4691	243.6075	⋯	2.575×10^{-2}	0.434	0.517	CO/He	
J1928+1458g (gpps0262)	19:28:42	+14:58	86.2	2.97268	18.3944	13.9841	⋯	8.678×10^{-3}	0.285	0.336	He	
J1928+1902g (gpps0163)	19:28:05	+19:02	28.9	5.79515	18.7472	20.0607	⋯	2.466×10^{-2}	0.427	0.508	CO	
J1929+1259g (gpps0345)	19:29:50	+12:59	90.9	2.85359	50.0942	23.8465	⋯	5.802×10^{-3}	0.245	0.288	He	
J1929+2355g (gpps0239)	19:29:44	+23:55	206.8	4.79296	10.1584	8.3292	⋯	6.012×10^{-3}	0.249	0.292	He	
J1930+1708g (gpps0274)	19:30:17	+17:08	87.2	2.27626	12.0134	7.3907	⋯	3.003×10^{-3}	0.193	0.226	He	
J1931+1428g (gpps0474)	19:31:48	+14:28	241.3	2.60770	0.1815	0.5682	⋯	5.979×10^{-3}	0.248	0.292	MS	Eclipse
J1936+1952g (gpps0065)	19:36:00	+19:52	325.3	9.72399	15.5908	8.5568	⋯	2.780×10^{-3}	0.187	0.219	He	
J1939+1848g (gpps0500)	19:39:01	+18:48	79.3	3.35659	11.9875	10.5015	⋯	8.653×10^{-3}	0.285	0.336	He	
J1940+2102g (gpps0564)	19:40:13	+21:02	76.3	30.04720	15.2938	31.2624	⋯	0.1403	0.889	1.086	CO/ONe	
J1943+2446g (gpps0434)	19:43:20	+24:46	237.3	5.59015	32.9876	11.2280	⋯	1.413×10^{-3}	0.147	0.171	He	
J1943+2847g (gpps0416)	19:43:36	+28:47	191.6	6.29597	12.9530	9.1491	⋯	4.901×10^{-3}	0.230	0.271	He	
J1952+2702g (gpps0054)	19:52:18	+27:02	213.1	4.14230	10.7125	8.1495	⋯	5.064×10^{-3}	0.233	0.274	He	
J1953+1006g (gpps0243)	19:53:34	+10:06	57.2	2.58559	0.1204	0.0225	⋯	8.437×10^{-7}	0.012	0.013	UL	Eclipse
J1957+2711g (gpps0562)	19:57:36	+27:11	210.4	23.37711	11.5406	24.7921	⋯	0.1228	0.838	1.020	CO	
J2000+3157g (gpps0590)	20:00:03	+31:57	270.0	3.49855	29.2071	18.2898	⋯	7.701×10^{-5}	0.273	0.321	He	
J2003+3032g (gpps0271)	20:03:53	+30:32	164.4	1.78537	0.1495	0.0677	⋯	1.491×10^{-5}	0.031	0.035	UL	
J2007+3343g (gpps0604)	20:07:53	+33:43	217.2	2.68151	1.8900	1.2175	⋯	5.425×10^{-4}	0.105	0.122	He	
J2015+3404g (gpps0544)	20:15:14	+34:04	208.0	4.27779	50.6152	26.4768	⋯	7.779×10^{-3}	0.274	0.322	He	

Notes: Pulsar name with the GPPS number in the bracket; right ascension (R.A., in hh:mm:ss.s); declination (decl., in dd:mm:ss.s), dispersion measure (DM, in pc cm^{-3}); pulsar spin period P (in millisecond); orbital period P_b (in days); projected semi-axis x (in light second); orbital eccentricity e; mass function f; the minimum and median companion mass $m_{c,min}$ and $m_{c,med}$ of the companion estimated by assuming the orbit inclination angle of $i = 90^{\circ}$ or 60° together with the pulsar mass $m_p = 1.35 M_{\odot}$; Companion types: He-white dwarf (He-WD), CO/ONe white dwarf (CO/ONe-WD), neutron star (NS), main sequence star (MS), ultra-light object or planet (UL); Notes: Eclipse for eclipsing pulsar.
References: (0): this work; (1): Yang et al. (2025a); (2): Su et al. (2024); (3): Yang et al. (2025b); (4): Pan et al. (2023).

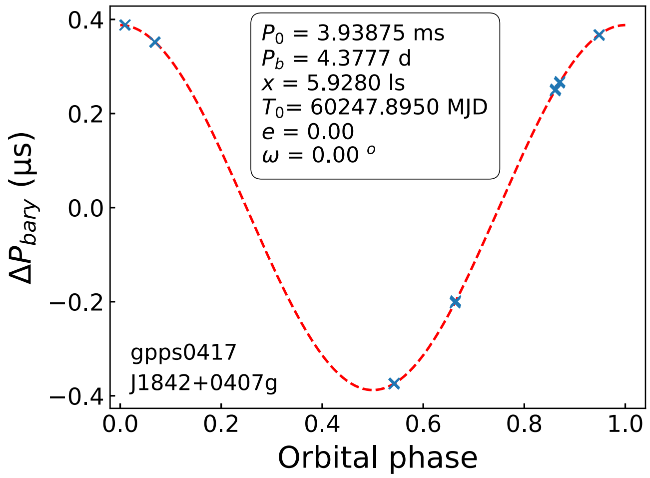

Figure 1. Variation of the barycentric periods for PSR J1842+0407g across the orbit phase. The observed barycentric periods are marked by "x" after the spin period P_0 is subtracted. The error bars are marked but too small to see for most data. The dashed line is the best-fit by using the preliminary Keplerian model with orbital parameters (P_b, x, T_0, e and ω) listed inside the panel. The orbital phase is referred to the periastron of the orbit. Plots for 78 newly discovered pulsars by the FAST GPPS survey are given in Figure A3 in the Appendix.

Moreover, relativistic deformation of the orbit (Weisberg & Huang 2016; Cameron et al. 2018) and relativistic spin–orbit coupling or named as Lense–Thirring process (Cameron et al. 2018; Hu et al. 2020; Venkatraman Krishnan et al. 2020) can also be detected from the change of orbital inclination.

Finding and precisely timing new binary systems, especially those with compact orbits, exceptional orbital configurations or the most massive pulsars, will improve the existing tests of gravity, the constraints of EOS and the understanding of the evolution channels of stellar binaries. There have been many efforts devoted to precise measurements of the binary nature of the systems (e.g., Deneva et al. 2021; Kramer et al. 2021; Miao et al. 2023), and most of them are follow-up observations of new pulsars discovered in large pulsar survey projects.

We are carrying out the Galactic Plane Pulsar Snapshot (GPPS) survey (Han et al. 2021) by using the Five-hundred-meter Aperture Spherical radio Telescope (FAST, Nan 2006; Nan et al. 2011), with a goal of discovering pulsars within the Galactic latitude of $\pm 10^\circ$ of the FAST visible sky area. Up to now, we have discovered 751 pulsars[10] (Han et al. 2025). Among them, about 160 pulsars show binary features, such as prominent acceleration in the discovery diagram or a significant variation of barycentric periods in the confirmation observation. We ascertain their binary nature with a few follow-up observations and get the orbital parameters determined for about 3/4 of them. More follow-up observations of these binary pulsars have been done by several applied FAST

[10] http://zmtt.bao.ac.cn/GPPS/GPPSnewPSR.html

Table 4
Measured and Derived Parameters of PSR J0528+3529, as One Example of 29 Pulsars with Phase-connected Timing Solutions Presented in Table A1

Pulsar Name	J0528+3529
GPPS name	gpps0537
MJD range	59930–60625
Data span (yr)	1.9
Number of TOAs	23
Ref. epoch (MJD)	60000
Measured quantities	
Right ascension: R.A. (hh:mm:ss)	05:28:28.7978(1)
Declination: decl. (dd:mm:ss)	+35:29:36.81(3)
Dispersion measure: DM (cm^{-3} pc)	111.837
Pulse frequency: ν (s^{-1})	12.78221930378(2)
First derivative ν: $\dot{\nu}$ (10^{-16} Hz s^{-1})	−1.202(4)
Residual (μs)	6.037
EFAC	0.77
EQUAD	0.0
Reduced χ^2	0.99
Binary parameters	
Binary model	DD
Orbital period: P_b (days)	11.7261813(4)
Projected semimajor axis: x (lt-s)	31.43468(2)
Periastron passage time: T_0 (MJD)	59994.190822(8)
Orbital eccentricity: e	0.2901088(10)
Longitude of periastron: ω (deg)	184.9436(2)
Advance rate of ω: $\dot{\omega}$ (deg yr^{-1})	0.0072(3)
Derived quantities	
Galactic longitude: l (deg)	172.52387(3)
Galactic latitude: b (deg)	0.46700(2)
YMW17[1] distance: D_{YMW} (kpc)	1.933
NE2001[2] distance: D_{NE2001} (kpc)	2.950
Spin period: P (ms)	78.23367572047(12)
Derivative of P: $\dot{P}$ (10^{-21} s s^{-1})	736(2)
Characteristic age: τ (Gyr)	1.686
Surface magnetic field: B_{surf} (10^8 G)	76.762

Note. Ephemeris obtained based on the DE440 solar system model (Park et al. 2021), Barycentric Dynamical Time (TDB) units, and TT(TAI) clock. Distances estimated by the YMW16 model (Yao et al. 2017) or NE2001 (Cordes & Lazio 2002).

projects, see Table 2. Combining all the data, we get timing solutions for some of them (see Table 3 and Table A1 in the Appendix). The first pulsar discovered by the GPPS survey, PSR J1901+0658 (gpps0001), is turned out to be a double NS system (Su et al. 2024). The 190th GPPS pulsar, PSR J1953+1844 (gpps0190), is a binary with the shortest orbital period of only 53 minutes (Pan et al. 2023), probably a descendant of an ultra-compact X-ray binary (Yang et al. 2023). PSR J1928+1815 (gpps0121) is an eclipsed MSP in a compact orbit with an orbital period of 3.6 hr, standing as evidence for the common envelope phase (Yang et al. 2025b). We get a timing

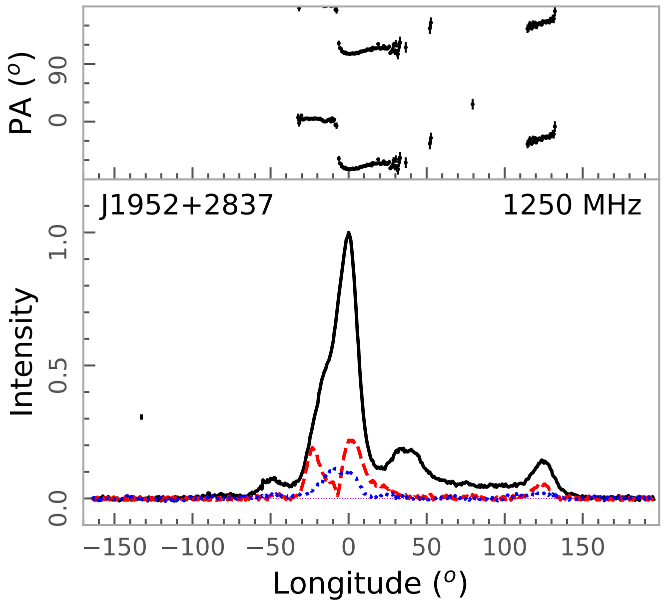

Figure 2. Integrated pulse profile of PSR J1952+2837. The total intensity, linear and circular polarization are represented by solid, dashed and dotted lines in the bottom sub-panel. The left-hand circular polarization is defined to be positive. The bin size and 3σ are marked inside the sub-panel, here σ is the standard deviation of off-pulse bins. In the top panel, dots with error bar are measurements of polarization position angles for linear polarization intensity exceeding 3σ line. The position angles are corrected to infinite frequency by discounting Faraday rotation. Polarized pulse profiles of the 29 pulsars are shown in Figure A2.

solution for six MSPs in compact orbits with massive WD companions (Yang et al. 2025a). Here, we present the results for 116 new binary pulsars, as listed in Table 3. In Section 2, we briefly describe the FAST observations and data reduction procedures. The Keplerian solutions and timing solutions are presented in Section 3 together with companion classification. Conclusions and further discussion are given in Section 4.

2. FAST Observations and Data Reduction

All FAST observations used in this paper (see Table 2) have been carried out by using the 19-beam *L*-band receiver. In the GPPS survey observations (ZD2020_2 to ZD2024_2), the snapshot observation mode has been used to cover a hexagonal sky area of 0.1575 square degrees by using 76 beams (see Figure 4 in Han et al. 2021). The follow-up observations have been carried out by using the tracking mode and also the 19-beam *L*-band receiver, including these verification observations made by the ZD202x_2 or the targeted observations by other free-applied projects (PT202x_0yyy).

The 19-beam *L*-band receiver works at a central frequency of 1250 MHz with a bandwidth of ~500 MHz (Jiang et al. 2020). Radio signals from two orthogonal linear polarizations, *X* and *Y*, are sampled, channelized and correlated (*XX*, *YY*, Re[X^*Y], Im[X^*Y]) in digital backends for each beam. The data stream are stored in "SEARCH MODE" PSRFITS files with 2048 spectral channels and a time resolution of 49.152 μs in our observations.

The GPPS survey observations take 5 minutes for each pointing (Han et al. 2021). The verification observations of a pulsar take 15 minutes for the targeted objects by using the central beam (M01) of the 19-beam *L*-band receiver if it has been detected in any survey beam. In tracking observations, the data from all 19 beams are also recorded. Sometimes we do detect some other pulsars from away beams (Han et al. 2025). In general, at the beginning or the end of each observation session, the periodic calibration noise signals are often turned on and off for 40 s or 1 minute or 2 minutes, which are used for the flux and polarization calibrations during off-line data processing.

2.1. Data Reduction

With the initial period and DM obtained from the GPPS survey, we fold the survey data and initial follow-up FAST observation data by using DSPSR[11] (van Straten & Bailes 2017). The optimal barycentric period $P_{\rm bary}$ for each observation is first searched from a set of trial periods around its nominal value by using the PDMP tool from PSRCHIVE[12] (Hotan et al. 2004). For a binary pulsar, the observed $P_{\rm bary}$ varies due to the Doppler effect caused by orbital motion (e.g., Freire et al. 2001). Its initial orbital parameters are obtained by grid searching over the two-dimensional parameter space of the orbital period $P_{\rm b}$ and the epoch of passage of periastron T_0, together with fitting for the projected semimajor axis x and spin period P_0. These parameters are further refined with FITORBIT,[13] during which the orbital eccentricity e and longitude of periastron ω might also be obtained. With this approach, preliminary orbital parameters are obtained for all the binaries systems, as shown in Figure 1 as an example. By combing orbital period $P_{\rm b}$ and projected semi-axis x, one can get the mass function f,

$$f(m_p, m_c) = \frac{(m_c \sin i)^3}{(m_p + m_c)^2} = \frac{4\pi^2 x^3}{T_\odot P_{\rm b}^2}. \quad (1)$$

Here, m_p and m_c are the masses for pulsar and the companion, i is the inclination angle of binary orbit, $T_\odot = GM_\odot/c^3 = 4.925490947\ \mu$s with G the gravitational constant and c the speed of light. Then the median companion masses can be obtained assuming $m_p = 1.35\ M_\odot$ and $\sin i = 60°$.

Some binary pulsars are monitored for years after initial discoveries by the GPPS survey. Further timing analysis is performed in the following steps. The ELL1 or DD model is

[11] http://dspsr.sourceforge.net/
[12] http://psrchive.sourceforge.net
[13] https://github.com/vivekvenkris/fitorbit

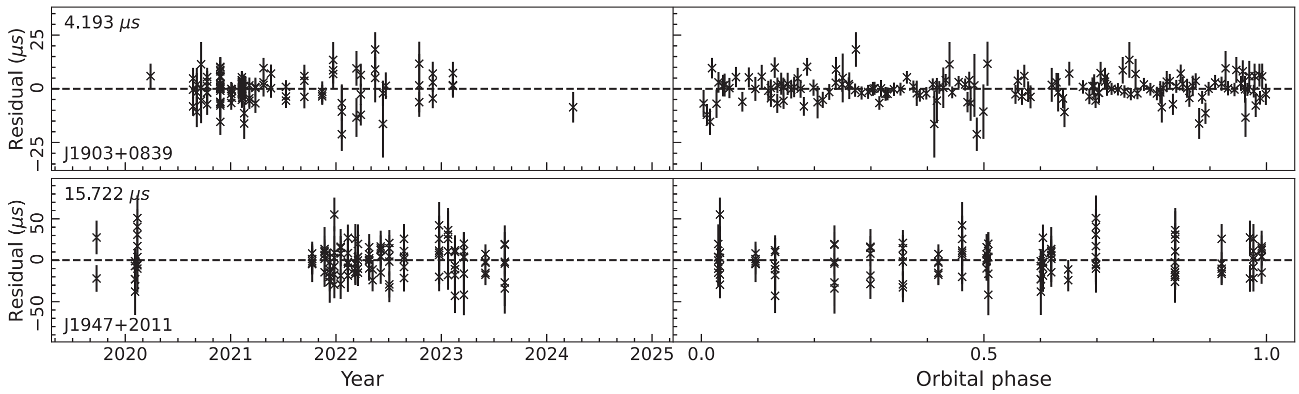

Figure 3. Timing residuals of two example pulsars PSR J1903+0839 and J1947+2011. Left panels: residuals vs. observation epochs. The weighted root-mean-square residual of each pulsar is indicated in the top left corner of the panel. Right panels: residuals vs. orbital phase. The orbital phases are referred to as ascending node or periastron depending on the binary model of each pulsar. Timing residuals of the 29 binary pulsars are shown in Figure A1.

Table 5
Polarization Profile Parameters of 29 New Binary Pulsars from Added FAST Observations Based on Pulsar Ephemeris

PSR	P (ms)	W_{50} (°)	W_{10} (°)	L/I (%)	V/I (%)	$\|V\|/I$ (%)	RM (rad m^{-2})
(1)	(2)	(3)	(4)	(5)	(6)	(7)	(8)
J0528+3529	78.233	6.6(7)	12.9(7)	10.2(31)	−5.0(31)	6.3(31)	−88(5)
J0622+0339	8.771	9.4(14)	⋯	49.7(38)	−13.4(36)	14.9(36)	28.9(15)
J1838+0024	5.087	92.2(28)	⋯	20.2(34)	1.7(34)	5.9(34)	52(9)
J1840+0012	5.338	193.7(14)	239.9(15)	36.2(31)	0.9(30)	6.9(31)	23.4(6)
J1844–0128	29.142	18(6)	⋯	⋯	−3(7)	4(7)	⋯
J1844+0028	3.571	61(3)	⋯	7.4(32)	9.2(32)	10.3(32)	−32(8)
J1845+0201	4.309	139(3)	156(3)	15.4(33)	−1.4(32)	5.1(32)	20(6)
J1845+0317	1.851	63.9(28)	⋯	80.1(43)	−1.6(38)	7.9(38)	20.2(16)
J1857+0642	3.530	42.0(7)	173.4(7)	34.1(30)	−8.6(30)	12.9(30)	−30.7(11)
J1903+0839	4.621	41.5(7)	216.2(7)	21.1(30)	5.9(30)	10.0(30)	247.1(13)
J1904+0553	4.907	40.9(7)	138.4(7)	12.8(30)	10.6(30)	12.3(30)	−67.0(16)
J1905+0649	27.464	20(3)	⋯	⋯	6(5)	8(5)	⋯
J1908+1036	10.690	5.5(7)	26.1(7)	71.3(31)	−1.0(30)	1.3(30)	−27.2(8)
J1911+1253	27.238	25.6(7)	38.8(7)	5.3(31)	4.2(31)	11.8(31)	224(7)
J1912+1416	3.166	50.8(14)	82.6(14)	15.1(31)	−7.2(31)	10.9(31)	214.7(24)
J1916+0740	11.219	91.8(14)	255.9(15)	15.9(31)	−10.6(31)	12.9(31)	609(3)
J1917+0615	3.967	73.5(14)	⋯	18.6(32)	−11.5(31)	14.9(31)	11.4(18)
J1917+1259	5.637	20.6(14)	⋯	9.8(33)	4.0(33)	10.9(33)	247(14)
J1918+0621	2.103	14.3(14)	34.5(14)	25.2(30)	26.6(30)	27.3(30)	−88.7(8)
J1924+1342	5.721	69.8(28)	⋯	14.9(33)	−12.6(31)	16.7(31)	103(13)
J1930+1403	3.209	25.1(14)	51.9(14)	42.5(31)	2.2(31)	2.4(31)	59.4(7)
J1932+2121	14.244	12.1(7)	36.6(7)	16.1(30)	−8.4(30)	9.5(30)	99.5(10)
J1936+2035	32.927	17.1(14)	⋯	64.4(38)	−0.7(37)	7.0(37)	12.7(12)
J1938+2302	52.761	11.2(7)	⋯	7.1(33)	−2.2(33)	4.0(33)	66(8)
J1943+2206	4.681	20(3)	⋯	20(4)	5(4)	11(4)	−165(25)
J1946+0904	25.772	30.7(7)	64.4(7)	19.8(30)	4.1(30)	5.0(30)	−105.3(6)
J1947+2011	8.177	9.1(7)	27.5(7)	7.8(32)	11.7(32)	13.6(32)	−48(8)
J1952+2837	18.020	21.1(7)	159.8(7)	21.4(30)	9.7(30)	11.2(30)	−42.5(5)
J2018+3518	31.316	20.3(28)	⋯	42.2(40)	5.7(35)	3.9(35)	−332(7)

Note. Numbers in brackets are uncertainties on the last digit. Columns (1)–(2): pulsar name; spin period, Columns (3)–(8): the profile properties: pulse widths W_{50} and W_{10} at 50% and 10% the peak intensities, degree (and uncertainty on the last digit) of linear, circular and absolute circular polarization L/I, V/I and $|V|/I$; FAST measured RM (and uncertainty), i.e., $\mathrm{RM} = \mathrm{RM_{obs}} - \mathrm{RM_{ion}}$.

Table 6
Population and Companion Statistics for Pulsar Binaries

Binary Pulsars	Known			FAST GPPS	
Total	420			116	
Location	GF	GC	EC	GF	GC
	315	104	1	115	1
He-WD	129	23	···	58	···
CO/ONe-WD	39	3	···	25	···
Ultra-light object	42	26	···	11	1
Main sequence star	22	5	1	5	···
Neutron star	17	2	···	3	···
Giant star	1	···	···	···	···
Helium star	···	···	···	1	···
uncertain	65	45	···	12	···

Note. GF, GC and EG stand for Galactic field, Globular clusters and extra galaxy, respectively. The known pulsar binaries are from ATNF pulsar Catalogue 2.4.0 (Manchester et al. 2005). It incorporates 3 triple systems with two having He-WD and one having UL companions.

first employed to model the orbital motion, depending on if xe^2 is much less or larger than the uncertainty of the time of arrival. Because one cannot reliably define the time and location of a periastron for a nearly circular orbit, the covariance can be avoided by the Laplace–Lagrange eccentricity parameterizations by using $\epsilon_1 = e \sin\omega$ and $\epsilon_2 = e \cos\omega$ (Lange et al. 2001). The ELL1 model is parameterized by $P_{\rm b}$, x, $T_{\rm asc}$, ϵ_1 and ϵ_2. Here, $T_{\rm asc} = T_0 - \omega P_{\rm b}/2\pi$ represents the epoch of the ascending node. The DD model is parameterized by $P_{\rm b}$, x, T_0, e and ω. These five Keplerian parameters of ELL1 or DD together with previously estimated pulsar position (α and δ), rotation period P and dispersion measure (DM) form the initial pulsar ephemeris.

With the initial ephemeris, we fold the data to form "FOLD MODE" PSRFITS archive files with DSPSR. After removing radio-frequency interference using PAZ and PSRZAP, one can integrate all subintegrations and all channels using PAM in the PSRCHIVE tool and get a noise-free standard profile template by using PAAS. Then, we obtain TOAs by cross-correlating the template with all observed pulse profiles by using PAT. With the initial ephemeride and TOAs, phase-coherent timing solution is obtained by determining the global rotational count by mapping the gaps between adjunct observations with DRACULA (Freire & Ridolfi 2018).

Using the phase-connected ephemeris, the recorded data are de-dispersed and folded again. They are calibrated in polarization following the procedures described by Wang et al. (2023). The whole frequency channels are summed to one for data every 5 minutes. New TOAs are extracted again. To account for the influence of white noise, ToA uncertainties are scaled

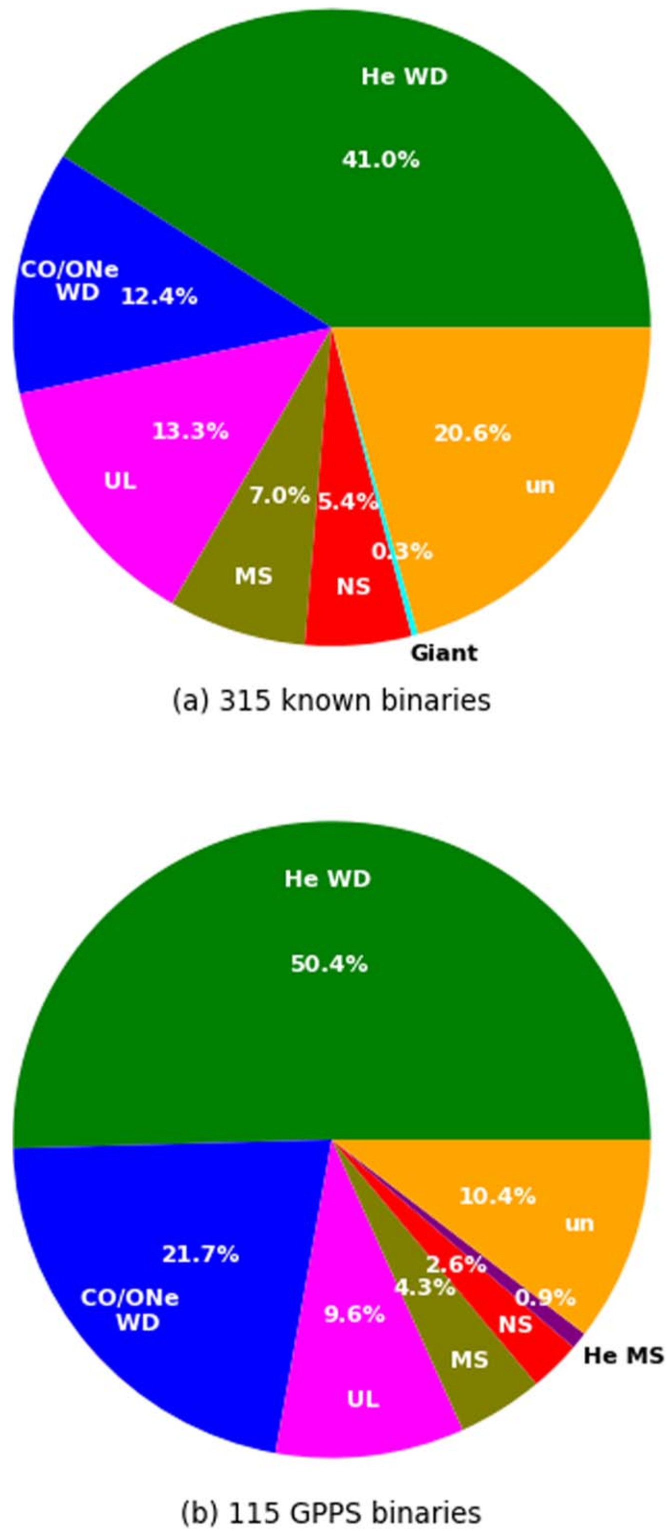

Figure 4. Fractions of binary pulsars with different types of companions in the Galactic field. The top panel is for 315 known binaries and the bottom panel is for the 115 GPPS-discovered ones. Their numbers are listed in Table 6.

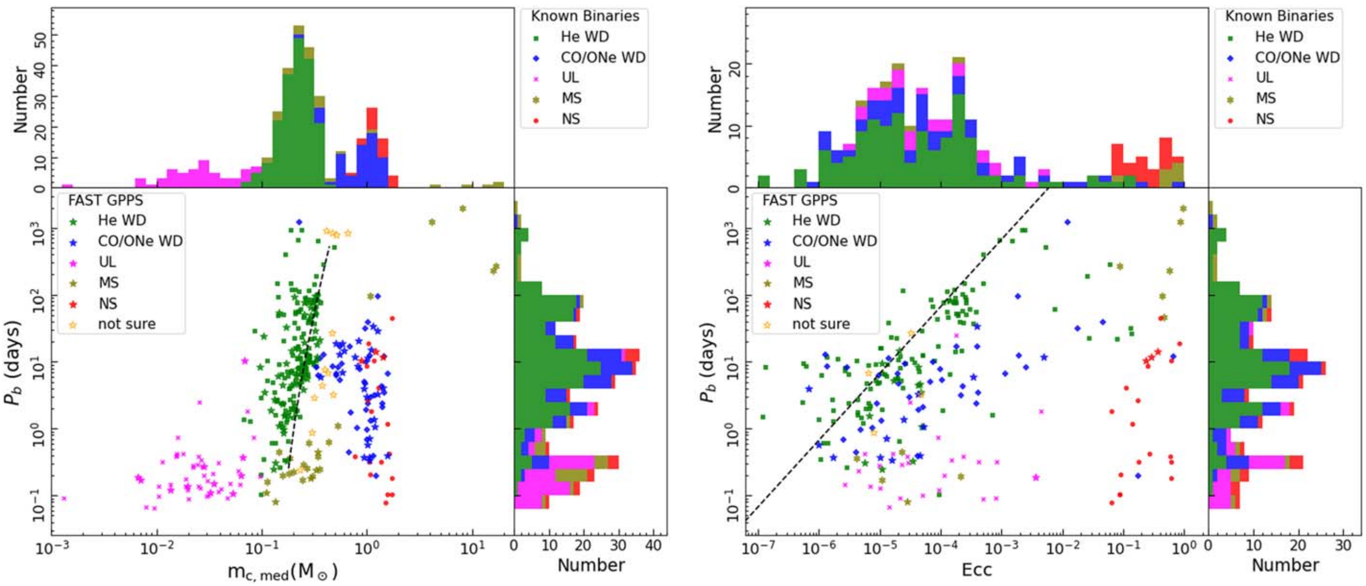

Figure 5. Binary parameters are clustered for various companion types. Binary parameters of previously known pulsars are taken from the ATNF pulsar catalog (www.atnf.csiro.au/people/pulsar/psrcat/ Manchester et al. 2005), plus the newly discovered binary pulsars by the FAST GPPS survey. In the main panel of the left plot, green squares, blue diamond, magenta crosses, olive asterisks and red dots represent the known He-WD, CO/ONe-WD, ultra-light (UL), main sequence star (MS) and neutron star (NS) companions, respectively. The binary pulsars reported in this work are represented by stars with colors for various companion types as the known ones and the orange for uncertain companion types. The dashed line is for neutron star—He-WD binaries predicted by Tauris & Savonije (1999). Histograms of the orbital period and companion mass are shown in the right and top panels for the sum of both the known and the new GPPS binaries with different types of companions. In the main panel of the right plot, the same data points for the orbital period vs. the orbit eccentricity are displayed. The dashed line represents the correlation between orbital period and eccentricity for MSP- He-WD systems as proposed by Phinney (1992). Histograms of the orbital period and eccentricity are shown in the right and top panels for the sum of known pulsars and GPPS pulsars.

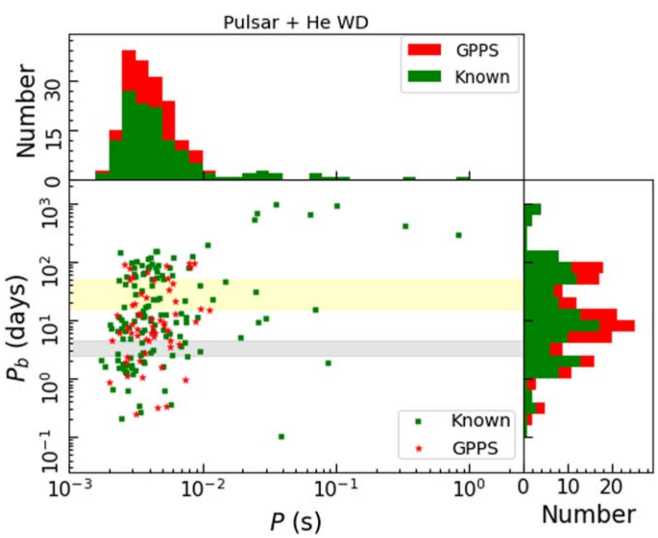

Figure 6. The distribution of pulsar periods and orbit periods for binary pulsars with He-WD companions. In the main panel, green dots represent the 129 known binary pulsars with He-WD companions in the Galactic field, the stars stand for the 58 GPPS pulsars with He-WD companions. The histograms on the top and right show the distributions of the pulsar spin period and orbital period.

by EFAC and quadratically added with EQUAD with the help of the efacEquad plugin of tempo2 (Hobbs et al. 2006). The ephemeris is finally refined to get a better parameter estimation with $\chi^2 \sim 1$. One example is given in Table 4, and the ephemeris of 29 pulsars in Table A1.

2.2. *Pulsar Polarization Profiles*

The polarized pulse profile represents the mean radiation feature of each pulsar. It is obtained by integrating the emission of tens of thousands of individual pulses. Data from multiple timing observations are then combined to form the integrated pulse profiles, as shown in Figure 2 for PSR J1952+2837 as an example. Polarization profiles for 29 pulsars are shown in Figure A2. The profile width at 50% and 10% the peak intensity, and the fractional linear, circular and absolute circular polarization are measured and listed in columns (3) to (7) of Table 5. The rotation measures (RM) are listed in column (8).

These pulsars are generally MSPs with wide profiles. The widths of their profiles range from $12\overset{\circ}{.}9$ to $255\overset{\circ}{.}9$ at 10% of the peak intensity. Profiles of PSRs J1840+0012 and J1916+0740 are extremely wide, emissions of which extend to more than

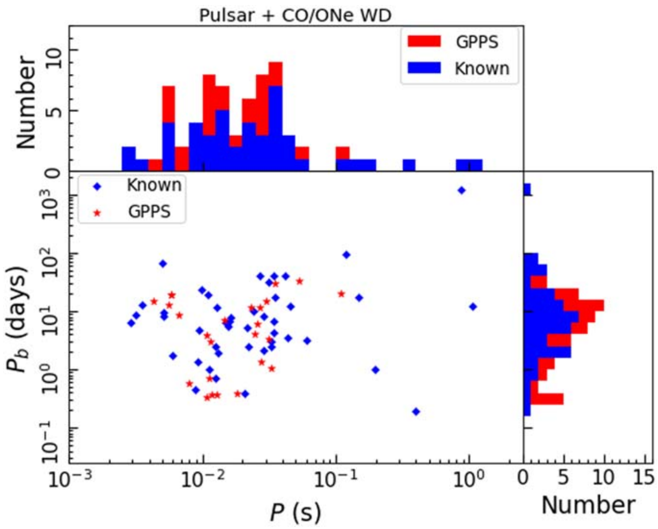

Figure 7. Distribution of pulsar spin periods and orbit periods of binaries with CO/ONe-WD companions. There are 39 known systems, plus 25 GPPS binary pulsars with a CO/ONe-WD companion.

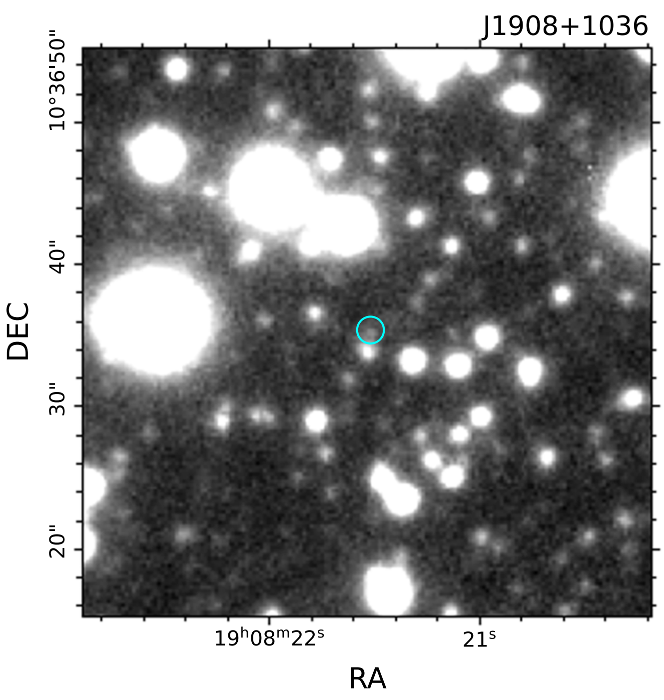

Figure 8. Optical images around the companion of PSR J1908+1036 from Pan-STRARRS1 (Chambers et al. 2016). The cyan circle is centered at the pulsar with a radius of one arcsecond.

180°. PSRs J1903+0839 and J1932+2121 exhibit inter-pulse emissions that separate by about 180° from the main pulses. PSRs J1840+0012, J1857+0642, J1916+0740, J1930+1403 and J1946+0904 have S-shaped position angle variations.

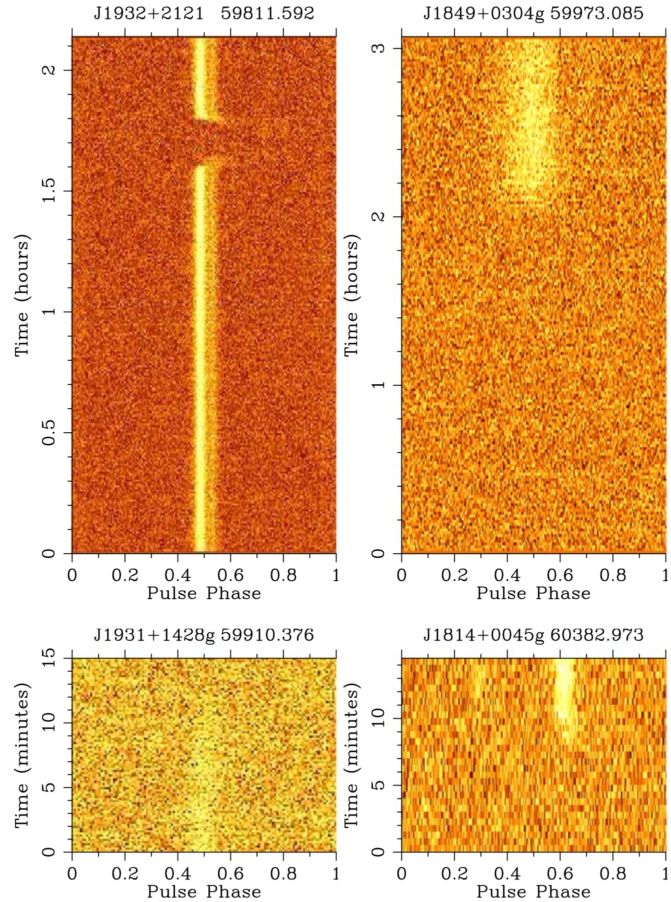

Figure 9. Eclipses of four binary pulsars. PSRs J1932+2121 and J1849+0304g are observed for 2.1 and 3.1 hr, PSRs J1931+1428g and J1814+0045g are observed for 15 minutes each.

PSRs J0528+3529, J1857+0642, J1903+0839, J1904+0553, J1916+0740, J1946+0904 and J1952+2837, exhibit orthogonal modes manifesting as 90° position angle jumps. The leading component of PSRs J1857+0642 and J1916+0740, the inter-pulse of PSR J1903+0839 and the profiles of PSRs J1845+0317 and J1908+1036 are highly linearly polarized. PSRs J1936+2035 and J2018+3518 are affected by interstellar scattering, which results in scattering tails of profiles together with flat PAs. These diverse polarization properties resemble those categories reported in Wang et al. (2023).

3. Detailed Results of Various Binary Pulsars

More than 160 binary pulsars have been found by the FAST GPPS survey. We have obtained nine pulsars published (Pan et al. 2023; Yang et al. 2023, 2025a, 2025b; Su et al. 2024), as mentioned at the end of the introduction. For 6 binary pulsars, PSRs J0653+0443, J1852–0044, J1856–0039, J1921+1631, J1922+1511 and J1933+2038, we have obtained the time solutions and are preparing independent papers. Here we list

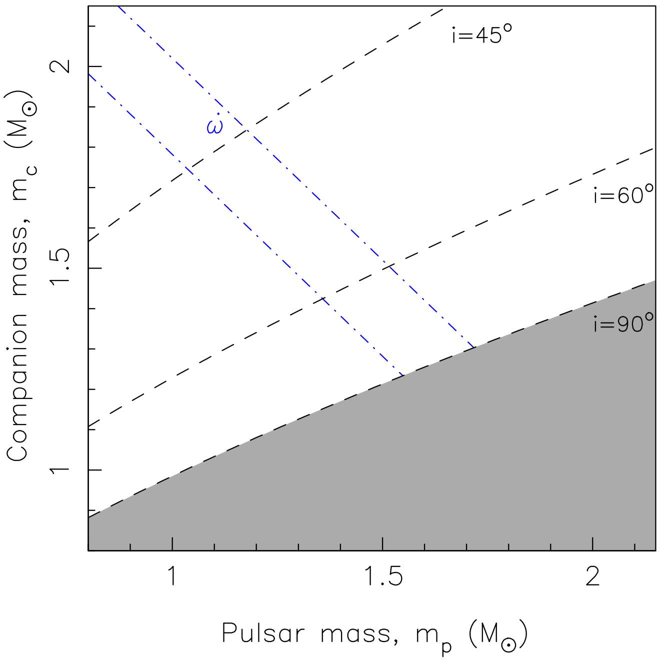

Figure 10. Mass–mass diagram of the double neutron star system PSR J0528+3529. The gray area represents the excluded parameter spaces from its mass function, with the boundary defined by an inclination angle of $i = 90°$. The area between two dashed–dotted blue lines is the possible parameter space, as constrained by the measured $\dot{\omega}$ within $\pm 1\sigma$.

116 pulsars in Table 3. The table consists of two parts, the first for pulsars with phase-connected timing solution, and the second part for pulsars without solutions. There are 38 pulsars in the first part, including the 9 published pulsars for completeness. For these 38 pulsars, we listed in the first part of Table 3 their names, R.A., Decl. and DM in columns (1), (2), (3) and (4). Spin period P obtained from discovery is refined from modeling the orbital motion, as listed in column (5). Columns (6), (7) and (8) are for orbital period $P_{\rm b}$, projected semi-axis x, and orbital eccentricity e obtained by modeling the Keplerian orbit. Mass functions of these binary systems are listed in column (9) of Table 3. By assuming $i = 90°$ or $60°$ and $m_p = 1.35 M_\odot$, the minimum and median companion mass are estimated, as listed in columns (10) and (11). With the spin period, orbital period, eccentricity and rough companion mass, the companion type can be roughly estimated, as listed in column (13) of Table 3. The new ephemeris with measured and derived parameters for 29 pulsars are given in detail in Appendix Table A1 and one example is shown in Table 4. The timing residuals are shown for two pulsars in Figure 3 and for all 29 pulsars in Figure A1, which are plotted along the observation epochs and versus the orbital phase. Timing residuals range from 1.053 to 174.563 μs.

For the other 78 pulsars, we have not yet obtained the timing solution from the limited number of observations, but we get the currently best-fitted preliminary Keplerian parameters obtained from available FAST observations made by the FAST GPPS survey or follow-up tracking observations in applied projects. Their positions have not been well determined yet, so their temporal names have "g" at the end.

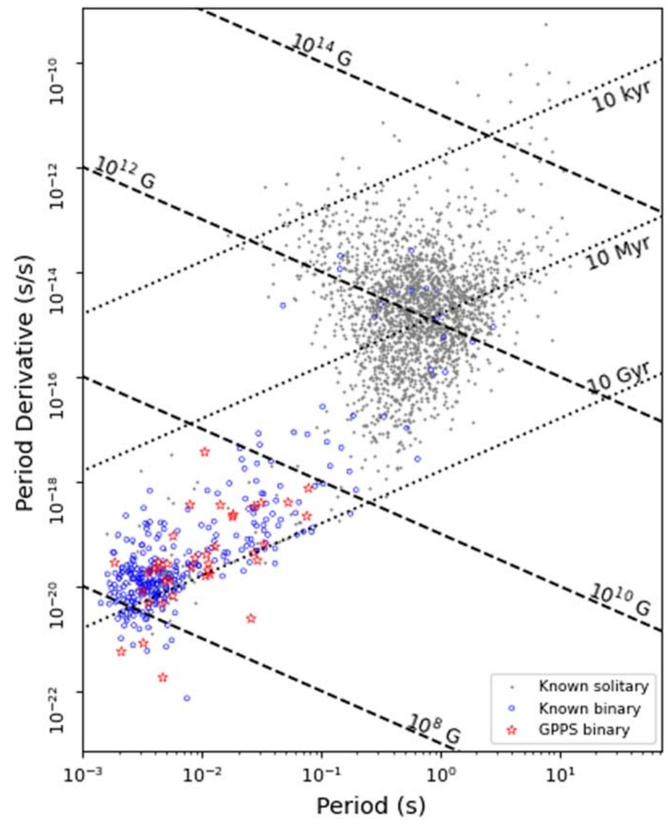

Figure 11. Binary pulsars in the period vs. period derivative diagram. Gray dots represent soliday single pulsars listed in the ATNF pulsar catalog (Manchester et al. 2005). Binary pulsars are indicated by circles. The newly discovered 38 binary pulsars by the GPPS survey which have timing solutions already are indicated by red stars. Dashed and dotted lines represent constant surface magnetic field and characteristic age, respectively.

The companions of binary pulsars are diverse (see Table 6). The ranges of the spin period (P), orbital period ($P_{\rm b}$), the estimated companion mass ($m_{\rm c,med}$) and orbital eccentricity (e) are listed in Table 1 for the binary pulsars with different types of companions in the Galactic field. Criteria for their classification are demonstrated in the last column. The companion type of a binary pulsar is determined based mainly on the measured P, $\dot{P}$, $P_{\rm b}$, $m_{\rm c,med}$ and e for a given binary system, as well as its distribution in the P_b versus $m_{\rm c,med}$ and $P_{\rm b}$ versus e diagrams, as shown in Figure 5.

See Table 6 for the numbers of the GPPS binary pulsars with various companions. Their fractions are shown in Figure 4. It is apparent that the GPPS binaries have a significantly larger fraction of He-WDs and CO-WDs compared with the known population.

Table 7
Kinematic Corrections of $\dot{P}$ and Relevant Parameters for 4 Pulsars with Proper Motion Measurement

Pulsar (1)	μ_T (mas yr^{-1}) (2)	$\dot{P}$ (10^{-21} s s^{-1}) (3)	$\dot{P}_S$ (10^{-21} s s^{-1}) (4)	$\dot{P}_G$ (10^{-21} s s^{-1}) (5)	$\dot{P}_I$ (10^{-21} s s^{-1}) (6)	$B_{\rm surf,c}$ (10^8 G) (7)	τ_c (Gyr) (8)	$\dot{E}_c$ (10^{33} erg s^{-1}) (9)
J1857+0642	5.9(9)	4.69	0.30	0.03	4.36	1.26	12.80	3.91
J1903+0839	5.0(9)	4.67	1.49	−1.78	4.96	1.53	14.74	1.98
J1904+0553	8.3(13)	12.75	3.65	−0.94	10.04	2.25	7.72	3.36
J1908+1036	12.0(22)	15.73	2.51	−0.03	13.25	3.81	12.75	0.43

Note. μ_T: total proper motion, $\dot{P}_S$: Shklovskii effect, $\dot{P}_G$: Galactic acceleration, $\dot{P}_I$: intrinsic period derivative, $B_{\rm surf,c}$: corrected surface magnetic field, τ_c: corrected age, $\dot{E}_c$: corrected energy loss rate.

In the following, we discuss the GPPS binary pulsars according to their probable companions.

3.1. Pulsars with He-WD Companions

The pulsar He-WD binary systems are generally believed to be formed from the LMXBs via the Case A RLO which results in a fully recycled pulsar in an orbital period shorter than one day, or via the Case B RLO which results in a fully or partially recycled pulsar with an orbital period in the ranging from one to a thousand days (e.g., Webbink et al. 1983; Tauris & Savonije 1999; Podsiadlowski et al. 2002; Tauris & van den Heuvel 2023). The pulsar He-WD binaries might also be evolved from the IMXBs when the Case A RLO is not initiated too late during the main sequence evolution of the donor star (e.g., Podsiadlowski et al. 2002). Binary pulsars evolving in this channel are fully recycled and have an orbital period between 3 and 20 days (Tauris 2011).

Pulsars with He-WD companions are generally fully recycled and hence have spin periods $P < 10$ ms with a lognormal distribution with the most probable spin period of about 3.5 ms, as shown in Figure 6. The orbital periods range from 0.1 day to several hundred days. According to the criteria listed in Table 1 and the one suggested by Tauris et al. (2012), the companion of a pulsar with spin period less than 10 ms is most likely a He-WD if the median mass is in the range of $0.08 M_\odot < m_{\rm c,med} < 0.356 M_\odot$ for a system with an orbital period of $P_b < 100$ days, or the median mass in the range of $0.08 M_\odot < m_{\rm c,med} < 0.5 M_\odot$ for a system with an orbital period of $P_b > 100$ days.

We get 58 GPPS binary pulsars that most likely have He-WD companions. We have obtained a timing solution for 14 such pulsars, but not yet for another 44 pulsars (see Table 3). Among these GPPS pulsars, five pulsars, PSRs J1840+0012, J1903+0839, J1912+1416, J1829–0235g and J1908+0705g, have orbital periods shorter than one day and exhibit no eclipsing as shown from observations. They are most likely formed via the Case A RLO from LMXBs. The other 53 MSPs have orbital periods longer than one day and are most likely formed via the Case B RLO from LMXBs.

During the evolution, the recycling process results in two fossil relations for the orbital parameters for MSPs if they have a low-mass companion with an orbital period $P_b \geqslant 1$ day. One is P_b versus m_c (Refsdal & Weigert 1971; Tauris & Savonije 1999; Antoniadis 2014; Istrate et al. 2014), as shown in Figure 5. The GPPS pulsars, e.g., PSRs J0622+0339, J1844+0028, J1904+0553, J1916+0740, J1917+0615, J1918+0621, J1930+1403 and J1947+2011, are around the relation, which is an indication for the companion type.

The other fossil relation is P_b versus e for He-WD binaries (Phinney 1992), as shown in Figure 5. Positive correlations between P_b and e are evident for pulsars with He companions with a correlation coefficient of 0.66. This correlation is related to tides resulting from density fluctuations in the convective envelope, and systems with wider orbits during the mass transfer prevent perfect circularization (Tauris & van den Heuvel 2023). The GPPS pulsars, e.g., J1857+0642, J1943+2206 and J1947+2011, are consistent with the relation.

The distribution of orbital periods was noticed to have two gaps around $P_b \sim 25-50$ days (e.g., Tauris 1996; Taam et al. 2000) and around $P_b \sim 2.5-4.5$ days (Hui et al. 2018). With the newly discovered GPPS binary pulsars, we see the peaks are enhanced, and the gaps are confirmed with the lower boundary for the large gap extending from 25 to about 16 days, as shown in Figure 6.

3.2. Pulsars with CO/ONe-WD Companions

A pulsar CO/ONe-WD binary system can be formed from an IMXB via the Case A RLO in small orbits that results in a fully recycled pulsar with an orbital period of 3–20 days (Podsiadlowski et al. 2002; Tauris et al. 2011), or via an early Case B RLO in a wider orbit that results in a partial recycled pulsar with an orbital period of 3–50 days (Podsiadlowski et al. 2002), or via the late Case B or Case C RLO and a common envelope in very wide orbits that result in a partial recycled pulsar with CO/ONe companion with an orbital period less than 20 days (Ivanova et al. 2013; Tauris & van den Heuvel 2023). In addition, there are also systems that might be formed from LMXBs via the late Case B RLO (Tauris & Savonije 1999), which leads to a slowly spinning pulsar in an extremely wide orbit with orbital periods $\gtrsim$ 800 days. The NS in such a system is only mildly recycled. Another possibility is that in an HMXB the star with a higher initial mass evolves into a massive WD instead of an NS due to mass ratio reversal (Kaspi et al. 2000). The NSs in these systems are non-recycled and their orbit is eccentric.

The companion of a pulsar is likely a CO/ONe-WD when the pulsar has an orbital eccentricity $e < 0.05$, an orbital period $P_b < 100$ days, together with the companion having the median mass $m_{c,med} > 0.356 M_\odot$, as set in Table 1 and suggested by Tauris et al. (2012).

We have 25 binary pulsars discovered in the GPPS survey which probably have CO/ONe-WD companions, as listed in Table 3. Timing solutions have been obtained for 13 of them, with six ones reported in Yang et al. (2025a). Figure 7 shows the distribution of these pulsars in P versus P_b diagram. It is apparent that the binary pulsars with CO companions have a broad range of spin periods from as low as 2.9 ms to about 1.1 s, and have a most probable orbital period of about 10 days.

Among these systems, PSR J1908+1036 has the smallest eccentricity among all the pulsar CO-WD binary systems, though with large measurement uncertainty. The pulsar has a small DM of 10.91 pc cm^{-3}, which indicates that it is a nearby system. We do find the optical counterpart of the companion simply by inspecting manually the images from the Pan-STARRS1 image cutout server[14] with stack image at $grizy_{P1}$ bands, as shown in Figure 8. The detailed evolution history needs to be further investigated.

3.3. Pulsars with Ultra-light Companions

Some pulsars have a UL companion with a median mass $m_{c,med} < 0.08 M_\odot$ (Manchester et al. 2005; Tauris et al. 2012). The UL companions are generally formed via the Case A RLO of LMXBs (Tauris & van den Heuvel 2023). Magnetic braking takes away their orbital momentum leading to compact orbits. Some of them, such as PSR J1953+1844 (Yang et al. 2023), undergo evolution from ultra-compact X-ray binaries, then to accreting X-ray MSPs, and finally to binary MSPs with compact orbit together with UL companions (Podsiadlowski et al. 2002; van Haaften et al. 2012; Guo et al. 2024).

12 GPPS-discovered pulsars, PSRs J0541+2959g, J1814+0045g, J1830–0106g, J1838+1507g, J1847+0342g, J1856+1000g, J1911+1206g, J1919+0126g, J1953+1006g, J2003+3032g, J1845+0317 and J1953+1844, likely have UL companions. These pulsars are fully recycled. PSRs J1814+0045g and J1953+1006g are black-widows exhibiting eclipsing, whose companions have median masses of 0.064 and 0.013 $M_\odot$. Eclipse around the egress of PSR J1814+0045g is detected in a short observation, as shown in Figure 9. While the signals are fully eclipsed for PSR J1953+1006g during observations. Others are black widow candidates. Companions of PSRs J1845+0317 and J1911+1206g are the lightest and are most likely planets.

3.4. Pulsars with Main Sequence Star Companions

A small number of pulsars have MS star companions with the median mass $m_{c,med} > 0.5 M_\odot$ and orbital period $P_b > 50$ days (Tauris et al. 2012). Some redback systems with $P_b \lesssim 1$ day and $m_c \sim 0.1-0.4\ M_\odot$ might also have low-mass MS companions that experienced irradiation-induced mass loss.

We have five GPPS binary pulsars which likely have MS companions, PSRs J1849+0304g, J1859+0313g, J1919+1502g, J1931+1428g and J1932+2121. They are redbacks, and have a companion with a median mass from $0.110 M_\odot$ to $0.339 M_\odot$ in compact orbits and exhibit eclipses. The eclipses of PSRs J1932+2121, J1849+0304g and J1931+1428g are shown in Figure 9, as revealed by FAST observations. The FAST observation of PSR J1932+2121 exhibits a full eclipse lasting for about 10 minutes which is about 8.6% of the orbital phase. During the ingress and egress, pulsar emission is gradually delayed due to the extra DM contributed by the eclipsing material. The egress of the eclipse has also been observed for PSR J1849+0304g. The eclipse around ingress is detected in some short observations of PSR J1931+1428g. Eclipses of PSRs J1859+0313g and J1919+1502g result in the non-detection of pulsar emission in several observations.

The eclipses can be observed at multiple wavelengths and are desired for careful investigation to understand the out-flowing material from the companion stars (e.g., Podsiadlowski 1991), the companion properties and the binary orbit (e.g., Main et al. 2018; Li et al. 2019; Yu et al. 2023), which is hard to include in this paper.

3.5. Pulsars with NS Companions

The double NS binary systems are generally formed from HMXBs through the Case BB RLO following a CE phase, which leads to mild or marginal recycling for the first-born NSs (Tauris et al. 2017). As summarized by Su et al. (2024), there have been about 28 double NS systems, 23 DNS in the Galactic field (including five DNS candidates: PSRs J1753–2240, J1755–2550, J1759+5036, J1906+0746, and J2150+3427) with an orbital period in the range from 0.078 to 50 days and an eccentricity in the range from 0.064 to 0.828 (Tauris et al. 2012).

In the discovery of the FAST GPPS survey, three binary pulsars, PSRs J0528+3529, J1844–0128 and J1901+0658, are most likely in DNS systems. PSR J1901+0658 is the first GPPS-discovered pulsar, and was reported in Su et al. (2024).

PSR J0528+3529 has a spin period of 78.2 ms and a period derivative of 7.36×10^{-19} s s^{-1}. It is in an elliptic orbit with a period of 11.73 days and an eccentricity of 0.29. The ephemeris

[14] http://ps1images.stsci.edu/cgi-bin/ps1cutouts

is presented in Table 4. Its companion is estimated to have a median mass of 1.42 $M_\odot$. The relatively large companion mass together with the large eccentricity indicates that the companion is most likely an NS. Our timing observations demonstrate that its periastron advances with $\dot{\omega}$ of 0.0072(3) deg yr^{-1} (see Table 4). According to general relativity, the rate of advance of the periastron is described by (Blandford & Teukolsky 1976; Damour & Deruelle 1985),

$$\dot{\omega} = 3T_\odot^{2/3}\left(\frac{P_{\rm b}}{2\pi}\right)^{-5/3}\frac{1}{1-e^2}(m_p+m_c)^{2/3}. \quad (2)$$

With which, the total mass of the system is estimated to be 2.90(12) $M_\odot$. The possible mass spaces for both the pulsar and its NS companion are shown in Figure 10.

PSR J1844–0128 has a spin period of 29.1 ms, and is in an eccentric orbit with a period of 10.6 days and an eccentricity of 0.235. Its companion is estimated to have a median mass of 0.876 $M_\odot$, as listed in Table 3. Its periastron advance is marginally detected with $\dot{\omega}$ of 0.0059(18) deg yr^{-1}, which indicates a total mass of 1.7(8) $M_\odot$.

3.6. Pulsars with a Helium MS Companion

PSR J1928+1815 is in a compact circular orbit with a companion with a median mass of 1.395$M_\odot$ and shows the eclipse near the conjunction phase. Yang et al. (2025b) suggested the companion to be a He main sequence star.

3.7. Pulsars with Undetermined Companions

The companion nature of a binary system discussed above is inferred based on previous knowledge. However, there are too many evolution channels, each with very uncertain parameters. There are some ambiguous parameter space between the NS He-WD binary and the NS CO-WD binary, or between the NS He-WD binary and the NS-MS binary, or between the NS CO-WD binary and the DNS binary. Such ambiguity is mainly caused by the unknown orbital inclination angle and the lack of companion observations at other wave bands. Among newly discovered binary pulsars by the FAST GPPS survey, 11 pulsars may have a companion of either a He-WD or CO-WD, and one pulsar has a companion of either He-WD or MS star.

PSRs J1838+0028g, J1842+0407g, J1857+0642, J1908+0949, J1917+1259 and J1943+2206 are fully recycled MSPs in orbits with periods of 3–27 days. The median masses of the companion are in the range of 0.32–0.48 $M_\odot$. Such systems are typical descendants from the IMXB Case A evolution channel, and their companions are either CO-WDs or He-WDs (Tauris 2011).

PSRs J1900+0213g, J1910+0423g, J1917+1046g and J1923+2022g are typical descendants of LMXBs but in orbit with periods as long as almost 900 days. It is then difficult to assess the companion to be a He-WD or CO-WD according to Tauris & Savonije (1999). PSR J1952+2837 has a companion mass large and beyond that predicted by the $P_{\rm b}$ versus $m_{\rm c}$ relationship for the typical He-WDs. Moreover, unlike typical descendants of LMXBs, PSR J1952+2837 is mildly recycled with a spin period of 18 ms which probably evolves from an IMXB. The median companion mass is 0.30 $M_\odot$, which cannot be a CO-WD unless its orbital inclination is sufficiently low. But if the companion is a He-WD, the formation channel for such a system is unclear.

PSRs J1857–0125g has an orbital period of 0.24 days and a median companion mass of $m_{\rm c,med} = 0.23M_\odot$. Such a low-mass companion might be a He-WD or an MS exhibiting as redback systems with feedback from the NS (Chen et al. 2013; Strader et al. 2019). Further observations are desired to determine the companion nature by uncovering the possible pulsar eclipses and orbital period variations.

4. Conclusions and Discussion

In this work, we report 116 binary pulsars discovered by the FAST GPPS survey. We have obtained the timing solutions of 38 binary pulsars measured, as indicated in the distribution in the P–$\dot{P}$ diagram in Figure 11. In addition to the timing solutions for nine pulsars published previously, we present the measured and derived parameters for 29 binary pulsars with phase-coherent timing solutions. For the other 78 pulsars, we have obtained the best-fitted Keplerian parameters of the binary orbits based on several FAST observations. Most of the binary systems need to be further timed in the future, so that precise spin and orbital parameters of the systems with preliminary Keplerian parameters can be obtained. The PK parameters of the relativistic systems can be measured and improved. For example, the possible Shapiro delay in tight systems requires long term monitoring with good cadence and observation sensitivity.

With currently available measurements, we see that the pulsar binary systems we discovered in the GPPS survey have a broad range of spin periods, orbital periods and eccentricity. Among 116 pulsars, 104 of them have spin period $P < 30$ ms; 30 GPPS binaries have orbital periods shorter than one day and two of them shorter than 0.1 day. The shortest is 53 minutes for the black widow pulsar PSR J1953+1844 (Pan et al. 2023). The observed $\dot{P}$ of PSR J1943+2206 is the smallest among all the binary pulsars reported in this work. The inferred surface magnetic field strength is only 2.95×10^7 G.

Most of these binary pulsars have nearly circular orbits with $e < 0.001$, with He- or CO/ONe-WD companions in general. We noticed that three pulsars, PSRs J0528+3529, J1844–0128 and J1901+0658 have orbital eccentricities $e > 0.1$. Because of the large companion masses, they are very likely double NS systems, or NS-WD systems in which the NS formed after the massive WD, or an NS-MS system with a newly born NS. For evolved DNS or NS-WD systems, the large eccentricity indicates that the second formed object is most likely a compact NS if a significant eccentricity remains from the second supernova explosion (Tauris & van den Heuvel 2023).

Among these binaries discovered by the FAST GPPS survey, 58 pulsars rotate with He-WD companions in the orbit, 25 pulsars with a CO/ONe-WD companion, 11 pulsars with a UL companion, five with an MS companion, three pulsars with an NS companion and one with a He star as companion. We have 12 pulsars with companions of unknown natures. Combining these GPPS binaries with those known ones, we get the largest binary sample in the Galactic field. The He-WD, CO/ONe-WD, UL, MS and NS systems have fractions of 43.5%, 14.9%, 12.3%, 6.3% and 4.7%, in total.

For these pulsars with timing solutions, we obtained polarization pulse profiles by combining multiple FAST observations. The Geometry parameters have been derived from the polarization position angle curves as fitted by the RVM model. An optical counterpart is found for the companion of PSR J1908+1036 from the Pan-STARRS survey. The non-detection reveals that He-WD companions are generally cool and old. Post-Keplerian parameter $\dot{\omega}$ has been measured for the double NS systems PSRs J0528+3529 and J1844–0128, from which the total mass of the systems are estimated to be $2.90(12)M_\odot$ and $1.7(8)M_\odot$.

For very nearby pulsars, it should be noted that the observed pulsar spin-down rate comprises its intrinsic term $\dot{P}_{\rm I}$ plus the contributions from the Shklovskii effect $\dot{P}_{\rm S}$ and the Galactic acceleration $\dot{P}_{\rm G}$, in the form of

$$\dot{P} = \dot{P}_{\rm I} + \dot{P}_{\rm S} + \dot{P}_{\rm G}. \quad (3)$$

The Shklovskii effect results from the increase of projected distance between pulsar and solar system barycenter when a pulsar moves, which leads to the increase of pulse period (Backer & Hellings 1986). The Shklovskii term, $\dot{P}_{\rm S}$, as indicated in column (4) in Table 7, contributes 32% of the measured $\dot{P}$ for PSR J1903+0839 as an example. In a differential Galactic potential, the acceleration between a pulsar and the solar system barycenter, i.e., the Galactic acceleration term, can be found in Nice & Taylor (1995). We list the influences of gravitational acceleration $\dot{P}_{\rm G}$ listed in column (5) of Table 7. They are generally negative except for PSR J1857+0642. Its influence on period derivatives is more than 38% for PSR J1903+0839 as an example. Both the Shklovskii effect and the Galactic acceleration term cannot be neglected in calculating the intrinsic $\dot{P}_{\rm I}$. With $\dot{P}_{\rm I}$, the surface magnetic field, characteristic age and spin-down energy loss rate are re-estimated, as listed in columns (7)–(9) of Table 7.

Acknowledgments

This work made use of the data from FAST (Five-hundred-meter Aperture Spherical radio Telescope)(https://cstr.cn/31116.02.FAST). FAST is a Chinese national mega-science facility, operated by the National Astronomical Observatories, Chinese Academy of Sciences. P.F.W. is supported by the National SKA program of China (No. 2020SKA0120200), the National Natural Science Foundation of China (No. 12133004), the Chinese Academy of Science (No. JZHKYPT-2021-06) and the National Key R&D Program of China (No. 2021YFA1600401 and 2021YFA1600400). J.L.H. is supported by the National Natural Science Foundation of China (No. 11988101, 12133004 and 11833009).

Appendix
Tables and Figures for a Large Sample of Binary Pulsars

In the main text of this paper, we give only one example of a timing solution. Here we present the timing solutions of 29 binary pulsars. Their ephemerides are listed in Table A1. All ephemerides obtained here are based on the DE440 solar system ephemeris

Table A1
Phase-coherent Timing Solutions of 29 Binary Pulsars

Pulsar Name	J0528+3529	J0622+0339	J1838+0024	J1840+0012	J1844–0128
GPPS number	gpps0537	gpps0388	gpps0107	gpps0146	gpps0555
MJD range	59930–60625	59645–60484	59082–60651	59188–60062	59321–60604
Data span (yr)	1.9	2.3	4.3	2.4	3.5
Number of TOAs	23	106	97	78	59
Ref. epoch (MJD)	60000	60000	59500	59500	60000
Measured quantities					
R.A. (hh:mm:ss)	05:28:28.7978(1)	06:22:19.4862(2)	18:38:23.3856(2)	18:40:49.2066(1)	18:44:20.995(2)
Decl. (dd:mm:ss)	+35:29:36.81(3)	+03:39:42.882(11)	+00:24:20.655(4)	+00:12:30.007(4)	−01:28:25.77(5)
DM (cm^{-3} pc)	111.837(6)	79.4186(10)	122.629(4)	100.840(3)	368.18(18)
ν (Hz)	12.78221930378(2)	114.00514689571(2)	196.57464150790(3)	187.30193394493(5)	34.31188264149(10)
$\dot{\nu}$ (10^{-16} Hz s^{-1})	–1.202(4)	–4.51(5)	–10.296(6)	–4.52(2)	−0.36(4)
Residual (μs)	6.037	5.244	17.218	12.660	154.288
EFAC	0.77	1.0	0.97	1.0	0.85
EQUAD	0.0	0.0	0.0	0.0	0.0
Reduced χ^2	0.99	1.10	1.00	1.07	1.07

Table A1
(Continued)

Pulsar Name	J0528+3529	J0622+0339	J1838+0024	J1840+0012	J1844–0128
Binary parameters					
Binary model	DD	ELL1	ELL1	ELL1	DD
P_b (days)	11.7261813(4)	9.54626602(4)	8.41501155(3)	0.3285676513(13)	10.6003185(14)
x (lt-s)	31.43468(2)	4.891818(7)	2.643652(4)	0.528904(3)	20.96779(6)
T_{asc} (MJD)	···	60003.173741(4)	59659.932588(2)	59188.3036687(12)	···
ϵ_1 (10^{-5})	···	–0.69(10)	–2.31(24)	–2.2(21)	···
ϵ_2 (10^{-5})	···	–0.80(40)	–3.46(24)	2.7(29)	···
T_0 (MJD)	59994.190822(8)	···	···	···	60001.62635(7)
e	0.2901088(10)	···	···	···	0.234949(5)
ω (deg)	184.9436(2)	···	···	···	255.699(3)
$\dot{\omega}$ (deg yr^{-1})	0.0072(3)	···	···	···	0.0059(18)
Derived quantities					
l (deg)	172.52387(3)	206.334480(3)	31.804718(1)	31.9063976(3)	30.812029(9)
b (deg)	0.46700(2)	−4.783911(2)	3.0880369(3)	2.4573192(4)	0.904356(14)
D_{YMW} (kpc)	1.933	1.786	4.080	3.514	5.791
D_{NE2001} (kpc)	2.950	2.585	3.355	2.941	6.560
P (ms)	78.23367572047(12)	8.771533805528(2)	5.0871261538575(6)	5.3389731698873(15)	29.14442236961(9)
$\dot{P}$ (10^{-21} s s^{-1})	736(2)	34.7(3)	26.64(2)	12.89(4)	31(4)
τ (Gyr)	1.686	4.008	3.027	6.569	15.001
B_{surf} (10^8 G)	76.762	5.583	3.726	2.654	9.588
e (10^{-5})	···	1.06(26)	4.17(24)	3.5(26)	···

Pulsar name	J1844+0028	J1845+0201	J1845+0317	J1857+0642	J1903+0839
GPPS number	gpps0109	gpps0547	gpps0566	gpps0236	gpps0100
MJD range	58852–60138	59768–60518	59993–60677	59425–60409	58936–60402
Data span (yr)	3.5	2.1	1.9	2.7	4.0
Number of TOAs	52	34	44	79	144
Ref. epoch (MJD)	59500	60000	60300	59500	59500
Measured quantities					
R.A. (hh:mm:ss)	18:44:37.3595(2)	18:45:03.07708(4)	18:45:22.8858(3)	18:57:58.6789(2)	19:03:51.84526(5)
Decl. (dd:mm:ss)	+00:28:12.582(8)	+02:01:49.363(6)	+03:17:18.587(11)	+06:42:30.656(2)	+08:39:17.1924(9)
DM (cm^{-3} pc)	181.094(4)	56.653(1)	77.257(4)	21.5853(7)	166.451(2)
ν (Hz)	280.05934666221(6)	232.0589209905(2)	540.3354363648(3)	283.20671122381(3)	216.39545569709(1)
$\dot{\nu}$ (10^{-16} Hz s^{-1})	–14.17(3)	–15.17(9)	-82.3(3)	–3.763(8)	–2.190(6)
PMRA (mas yr^{-1})	···	···	···	5.7(9)	–4.9(9)
PMDEC (mas yr^{-1})	···	···	···	1.6(10)	1.2(13)
Residual (μs)	17.199	2.082	10.844	2.506	4.193
EFAC	1.0	1.0	1.0	1.0	1.0
EQUAD	0.0	0.0	0.0	1.2	2.0
Reduced χ^2	1.11	1.22	1.00	1.23	1.19
Binary parameters					
Binary model	ELL1	ELL1	ELL1	ELL1	ELL1
P_b (days)	1.078895359(3)	5.32570888(3)	0.19009980(3)	6.734521817(6)	0.3126397707(3)
x (lt-s)	1.059555(5)	4.551805(2)	0.015146(5)	8.782903(3)	0.4050089(6)
T_{asc} (MJD)	59570.1860995(13)	60002.988523(2)	60300.12080(3)	59902.1721621(1)	59179.2317147(1)
ϵ_1 (10^{-5})	1.2(11)	0.72(18)	297(139)	–0.53(5)	0.56(29)
ϵ_2 (10^{-5})	–4.7(27)	1.55(8)	216(80)	–0.39(3)	–0.10(36)
Derived quantities					
l (deg)	32.573422(3)	34.012031(2)	35.171174(4)	39.6471272(9)	42.0453999(3)
b (deg)	1.7307459(3)	2.3462112(6)	2.8450204(1)	1.6072138(5)	1.19956909(7)

Table A1
(Continued)

Pulsar name	J1844+0028	J1845+0201	J1845+0317	J1857+0642	J1903+0839
$D_{\rm YMW}$ (kpc)	4.565	1.669	2.799	0.994	5.317
$D_{\rm NE2001}$ (kpc)	5.015	2.251	2.770	1.586	4.861
P (ms)	3.5706717591045(8)	4.309250408179(3)	1.8507022354998(9)	3.5309897695529(4)	4.6211691312030(2)
$\dot{P}$ (10^{-21} s s^{-1})	18.07(4)	28.2(2)	28.20(9)	4.69(1)	4.67(2)
τ (Gyr)	3.133	2.425	1.041	11.93	15.66
$B_{\rm surf}$ (10^8 G)	2.571	3.526	2.312	1.30	1.48
e (10^{-5})	4.9(26)	1.7(1)	367(122)	0.66(4)	0.56(29)

Pulsar name	J1904+0553	J1905+0649	J1908+1036	J1911+1253	J1912+1416
GPPS number	gpps0039	gpps0229	gpps0114	gpps0181	gpps0169
MJD range	58898–59753	58897– 60237	58989–60348	59271–60348	59256–60231
Data span (yr)	2.4	3.7	3.7	3.0	2.7
Number of TOAs	88	37	131	90	44
Ref. epoch (MJD)	59500	59500	59500	59500	59500
Measured quantities					
R.A. (hh:mm:ss)	19:04:16.82283(4)	19:05:05.2578(13)	19:08:21.5212(2)	19:11:28.6990(2)	19:12:30.51373(5)
Decl.(dd:mm:ss)	+05:53:53.6127(9)	+06:49:49.33(5)	+10:36:35.368(4)	+12:53:17.414(5)	+14:16:23.674(2)
DM (cm^{-3} pc)	164.275(2)	187.67(2)	10.915(3)	68.689(4)	66.665(1)
ν (Hz)	203.77706071885(2)	36.41075526203(4)	93.54365951465(1)	36.71246645742(1)	315.83188917471(4)
$\dot{\nu}$ (10^{-16} Hz s^{-1})	–5.296(8)	–4.43(3)	–1.376(5)	–0.583(4)	–8.039(13)
PMRA (mas yr^{-1})	–5.5(6)	…	–6.7(11)	…	…
PMDEC (mas yr^{-1})	–6.2(17)	…	–9.9(26)	…	…
px	4.5(17)	…	…	…	…
Residual (μs)	3.328	75.868	14.217	20.105	3.976
EFAC	1.0	1.0	1.6	0.74	1.0
EQUAD	0.0	0.0	2.4	0.0	0.0
Reduced χ^2	1.24	0.75	1.15	1.14	1.21
Binary parameters					
Binary model	ELL1	ELL1	ELL1	DD	ELL1
$P_{\rm b}$ (days)	1.583625978(2)	1.381714792(2)	3.964125977(2)	11.78905319(2)	0.2468944916(2)
x (lt-s)	1.4177437(9)	6.62159(5)	11.388257(3)	20.437275(5)	0.329811(2)
$T_{\rm asc}$ (MJD)	59133.6085907(3)	59006.799191(2)	59595.0312387(3)	…	59570.1674523(3)
ϵ_1 (10^{-5})	–0.56(10)	1.9(20)	–0.027(74)	…	–0.4(16)
ϵ_2 (10^{-5})	0.36(13)	−1.6(16)	–0.063(66)	…	–1.0(12)
T_0 (MJD)	…	…	…	59664.9707(2)	…
e	…	…	…	0.0050267(5)	…
ω (deg)	…	…	…	250.479(6)	…
Derived quantities					
l (deg)	39.6428450(3)	40.56309(3)	44.291270(2)	46.665604(1)	48.0101799(5)
b (deg)	–0.15604912(3)	0.093482(2)	1.1132798(3)	1.4864690(1)	1.90457045(8)
$D_{\rm YMW}$ (kpc)	4.438	4.370	0.671	2.164	2.166
$D_{\rm NE2001}$ (kpc)	4.498	4.891	0.593	3.335	3.354
P (ms)	4.9073237020514(4)	27.46441244636(3)	10.690195414509(2)	27.238703810866(9)	3.1662413906749(4)
$\dot{P}$ (10^{-21} s s^{-1})	12.75(2)	334(2)	15.73(6)	43.3(3)	8.06(2)
τ (Gyr)	6.10	1.305	10.775	9.97	6.229
$B_{\rm surf}$ (10^8 G)	2.53	30.64	4.14	10.99	1.617
e (10^{-5})	0.67(11)	2.5(19)	0.069(68)	…	1.1(12)

Pulsar name	J1916+0740	J1917+0615	J1917+1259	J1918+0621	J1924+1342
GPPS number	gpps0166	gpps0460	gpps0012	gpps0494	gpps0032
MJD range	59263–60403	58713–60453	58770–59985	58713–60344	58989–60518
Data span (yr)	3.1	4.8	3.3	4.5	4.2
Number of TOAs	118	39	79	94	35
Ref. epoch (MJD)	59500	59500	59500	59500	59500

Table A1
(Continued)

Pulsar name	J1916+0740	J1917+0615	J1917+1259	J1918+0621	J1924+1342
Measured quantities					
R.A. (hh:mm:ss)	19:16:15.4327(7)	19:17:20.2887(2)	19:17:21.3371(2)	19:18:00.6061(13)	19:24:16.5972(4)
Decl. (dd:mm:ss)	+07:40:41.175(11)	+06:15:29.192(3)	+12:59:59.822(3)	+06:21:59.38(5)	+13:42:50.076(12)
DM (cm^{-3} pc)	219.86(2)	172.474(4)	117.017(4)	63.1179(3)	98.347(9)
ν (Hz)	89.1292592477(1)	252.03522036226(7)	177.38458504550(4)	475.3568747441(6)	174.7919902256(2)
$\dot{\nu}$ (10^{-16} Hz s^{-1})	–1.59(4)	–13.42(3)	–2.06(2)	–1.26(10)	–27.44(4)
Residual (μs)	73.8	8.133	15.451	1.053	28.919
EFAC	0.93	1.0	1.0	1.0	1.0
EQUAD	0.0	0.0	0.0	0.0	0.0
Reduced χ^2	1.10	0.95	1.48	0.85	1.02
Binary parameters					
Binary model…	ELL1	ELL1	ELL1	ELL1	ELL1
P_b (days)	14.8184145(3)	4.61843740(3)	3.201264482(5)	4.44919663(8)	3.5281740(2)
x (lt-s)	7.315593(13)	3.55159(2)	5.896282(6)	2.73700(3)	1.60733(1)
T_{asc} (MJD)	59557.237288(6)	60000.264924(2)	58890.9075574(7)	59899.843887(4)	59201.118335(4)
ϵ_1 (10^{-5})	2.07(61)	2.8(3)	–4.75(16)	2.2(12)	–2.5(16)
ϵ_2 (10^{-5})	0.30(34)	–3.6(11)	–0.70(13)	–3.5(18)	–4.0(30)
Derived quantities					
l (deg)	42.594803(4)	41.461307(1)	47.429743(1)	41.635129(5)	48.851147(3)
b (deg)	–1.971786(1)	–2.8694721(4)	0.2701915(4)	–2.966894(2)	–0.8802052(2)
D_{YMW} (kpc)	8.434	8.159	3.642	1.948	3.040
D_{NE2001} (kpc)	6.213	5.407	4.273	2.893	4.082
P (ms)	11.21966017041(2)	3.967699429321(1)	5.637468440357(1)	2.103682629053(3)	5.721085953135(6)
$\dot{P}$ (10^{-21} s s^{-1})	20.0(5)	21.12(4)	6.54(5)	0.56(5)	89.83(13)
τ (Gyr)	8.87	2.977	13.65	59.854	1.010
B_{surf} (10^8 G)	4.79	2.930	1.94	0.346	7.254
e (10^{-5})	2.10(60)	4.6(9)	4.80(16)	4.2(16)	4.8(26)

Pulsar name	J1930+1403	J1932+2121	J1936+2035	J1938+2302	J1943+2206
GPPS number	gpps0013	gpps0403	gpps0197	gpps0392	gpps0514
MJD range	58808-60408	59661–60254	58901–60257	59654–60392	59380–60540
Data span (yr)	4.3	1.6	3.7	2.0	3.2
Number of TOAs	90	91	57	277	166
Ref. epoch (MJD)	59500	59500	59500	60000	59500
Measured quantities					
R.A. (hh:mm:ss)	19:30:17.62052(5)	19:32:21.2014(2)	19:36:38.3072(7)	19:38:11.6306(4)	19:43:43.6485(3)
Decl. (dd:mm:ss)	+14:03:53.8022(7)	+21:21:06.786(2)	+20:35:47.29(2)	+23:02:00.164(5)	+22:06:33.261(7)
DM (cm^{-3} pc)	150.487(3)	192.101(1)	198.86(3)	303.365(8)	211.100(7)
ν (Hz)	311.58002361009(2)	70.20153107379(3)	30.36958214096(3)	18.953122076237(7)	213.59893407472(14)
$\dot{\nu}$ (10^{-16} Hz s^{-1})	–0.792(5)	–17.37(2)	–0.58(2)	–1.421(6)	–0.08(3)
Residual (μs)	4.853	6.881	91.590	71.615	33.591
EFAC	1.0	1.0	1.0	1.0	1.0
EQUAD	1.4	0.0	0.0	0.0	0.0
Reduced χ^2	1.03	1.21	1.35	0.91	0.97
Binary parameters					
Binary model	ELL1	ELL1	ELL1	DD	ELL1
P_b (days)	5.574928410(4)	0.0809057967(2)	1.064143467(4)	33.9698770(2)	26.76246566(9)
x (lt-s)	5.180409(2)	0.1626938(15)	5.64685(2)	54.670805(9)	23.79641(2)
T_{asc} (MJD)	59216.6227321(3)	59688.9941818(3)	59495.651756(1)	…	59003.294385(4)
ϵ_1 (10^{-5})	0.35(4)	2.0(16)	–1.1(11)	…	0.77(6)
ϵ_2 (10^{-5})	1.88(4)	–2.0(14)	5.2(9)	…	–3.17(12)

Table A1
(Continued)

Pulsar name	J1930+1403	J1932+2121	J1936+2035	J1938+2302	J1943+2206
T_0 (MJD)	⋯	⋯	⋯	59976.131(5)	⋯
e	⋯	⋯	⋯	0.0004038(3)	⋯
ω (deg)	⋯	⋯	⋯	324.53(5)	⋯
Derived quantities					
l (deg)	49.8554128(3)	56.4805218(9)	56.305424(6)	58.607434(2)	58.435492(2)
b (deg)	–1.99723150(8)	1.0786393(4)	–0.1625533(3)	0.7148274(7)	–0.85242037(4)
$D_{\rm YMW}$ (kpc)	4.733	5.106	4.992	8.945	7.991
$D_{\rm NE2001}$ (kpc)	5.374	6.612	6.668	9.145	7.262
P (ms)	3.2094483735304(2)	14.244703565637(6)	32.92768386995(3)	52.76175587207(2)	4.681671302958(3)
$\dot{P}$ (10^{-21} s s^{-1})	0.815(5)	352.5(4)	62.7(17)	395(2)	0.18(6)
τ (Gyr)	62.37	0.641	8.323	2.115	407.65
$B_{\rm surf}$ (10^8 G)	0.51	22.676	14.539	46.222	0.295
e (10^{-5})	1.91(4)	2.8(15)	5.3(9)	⋯	3.26(12)

Pulsar name	J1946+0904	J1947+2011	J1952+2837	J2018+3518
GPPS number	gpps0242	gpps0011	gpps0064	gpps0393
MJD range	59413–60545	58749–60165	58852–60624	59633–60045
Data span (yr)	3.1	3.9	4.9	1.1
Number of TOAs	35	125	126	83
Ref. epoch (MJD)	60000	59500	59500	60000
Measured quantities				
R.A. (hh:mm:ss)	19:46:56.8707(2)	19:47:47.71374(9)	19:52:49.65344(5)	20:18:48.149(7)
Decl. (dd:mm:ss)	+09:04:53.337(8)	+20:11:00.454(2)	+28:37:12.9120(9)	+35:18:45.85(5)
DM (cm^{-3} pc)	37.186(4)	127.495(3)	313.112(3)	266.994(22)
ν (Hz)	38.801408988633(8)	122.285985983522(9)	55.490992750915(3)	31.932334792(1)
$\dot{\nu}$ (10^{-16} Hz s^{-1})	–0.036(6)	−3.464(4)	−6.5075(8)	–4.0(8)
Residual (μs)	6.490	15.722	5.908	174.563
EFAC	0.7	1.0	1.4	1.0
EQUAD	0.0	5.0	0.6	0.0
Reduced χ^2	1.07	1.05	1.05	1.35
Binary parameters				
Binary model	DD	DD	ELL1	ELL1
$P_{\rm b}$ (days)	6.037962681(10)	81.9689107(3)	0.8674946510(4)	3.3327156(1)
x (lt-s)	7.135242(5)	37.803932(3)	1.662420(3)	12.44297(5)
$T_{\rm asc}$ (MJD)	⋯	⋯	59415.77258787(8)	59969.165234(3)
ϵ_1 (10^{-5})	⋯	⋯	−0.39(18)	3.4(7)
ϵ_2 (10^{-5})	⋯	⋯	−0.21(16)	2.7(10)
T_0 (MJD)	59999.719(4)	59653.646(14)	⋯	⋯
e	0.000344(3)	0.0001401(2)	⋯	⋯
ω (deg)	335.59(22)	175.86(6)	⋯	⋯
Derived quantities				
l (deg)	47.462644(2)	57.2431035(7)	65.0916910(4)	73.69187(3)
b (deg)	–7.9791543(4)	−2.63783970(3)	0.6671998(2)	−0.37868(1)
$D_{\rm YMW}$ (kpc)	1.604	4.287	10.474	7.077
$D_{\rm NE2001}$ (kpc)	2.155	5.108	9.722	8.435
P (ms)	25.772259978831(5)	8.1775519243451(6)	18.0209426868383(8)	31.316219328(1)
$\dot{P}$ (10^{-21} s s^{-1})	2.4(4)	23.17(3)	211.33(3)	388(80)
τ (Gyr)	171.58	5.59	1.35	1.279
$B_{\rm surf}$ (10^8 G)	2.507	4.40	19.75	35.283
e (10^{-5})	⋯	⋯	0.44(17)	4.3(8)

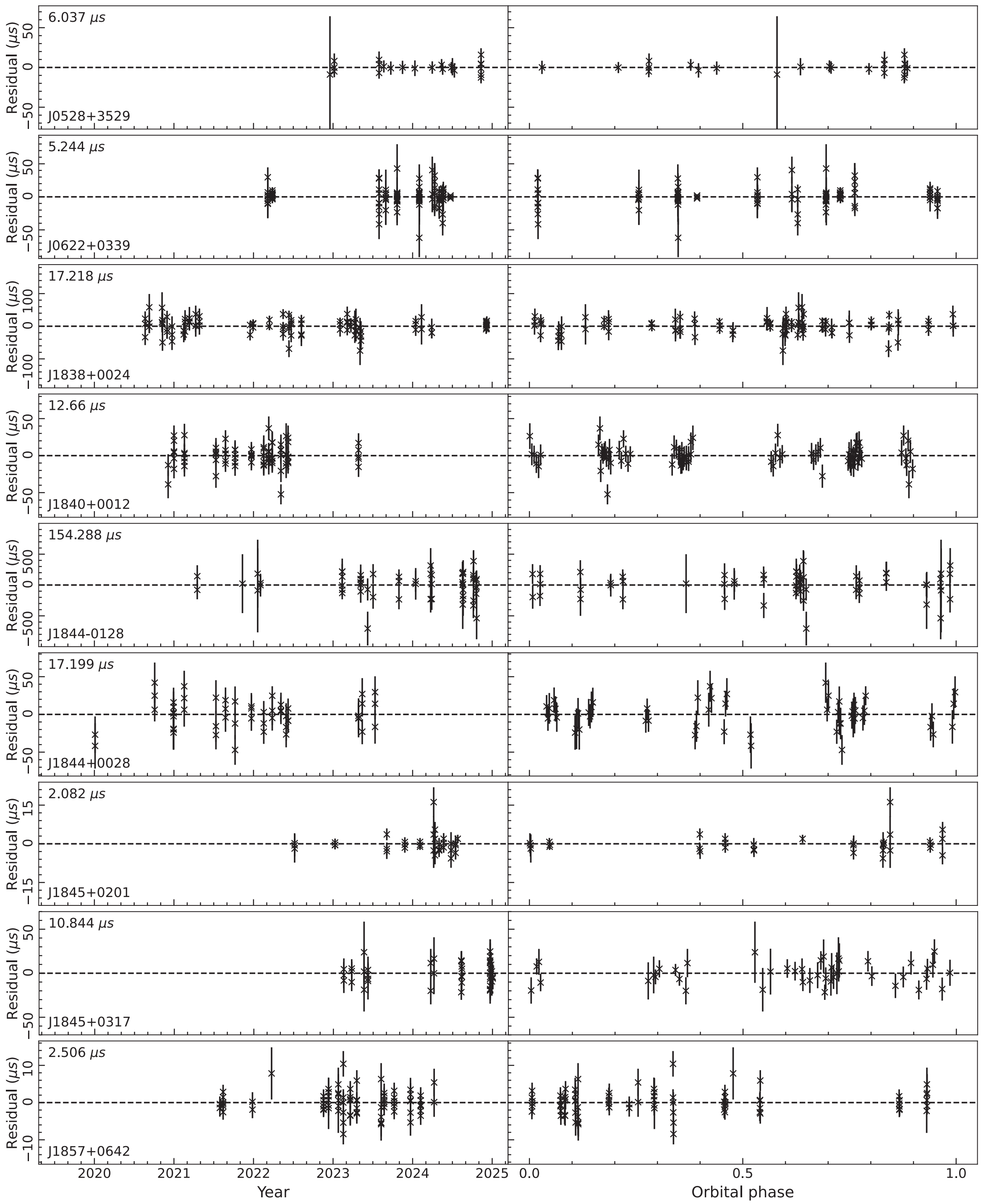

Figure A1. Timing residuals of 29 newly discovered binary pulsars by the FAST GPPS survey. Left panels: residuals vs. observation epochs. The weighted root-mean-square residual of each pulsar is indicated in the top right corner of the panel. Right panels: residuals vs. orbital phase. The orbital phases are referred to as ascending node or periastron depending on the binary model of each pulsar.

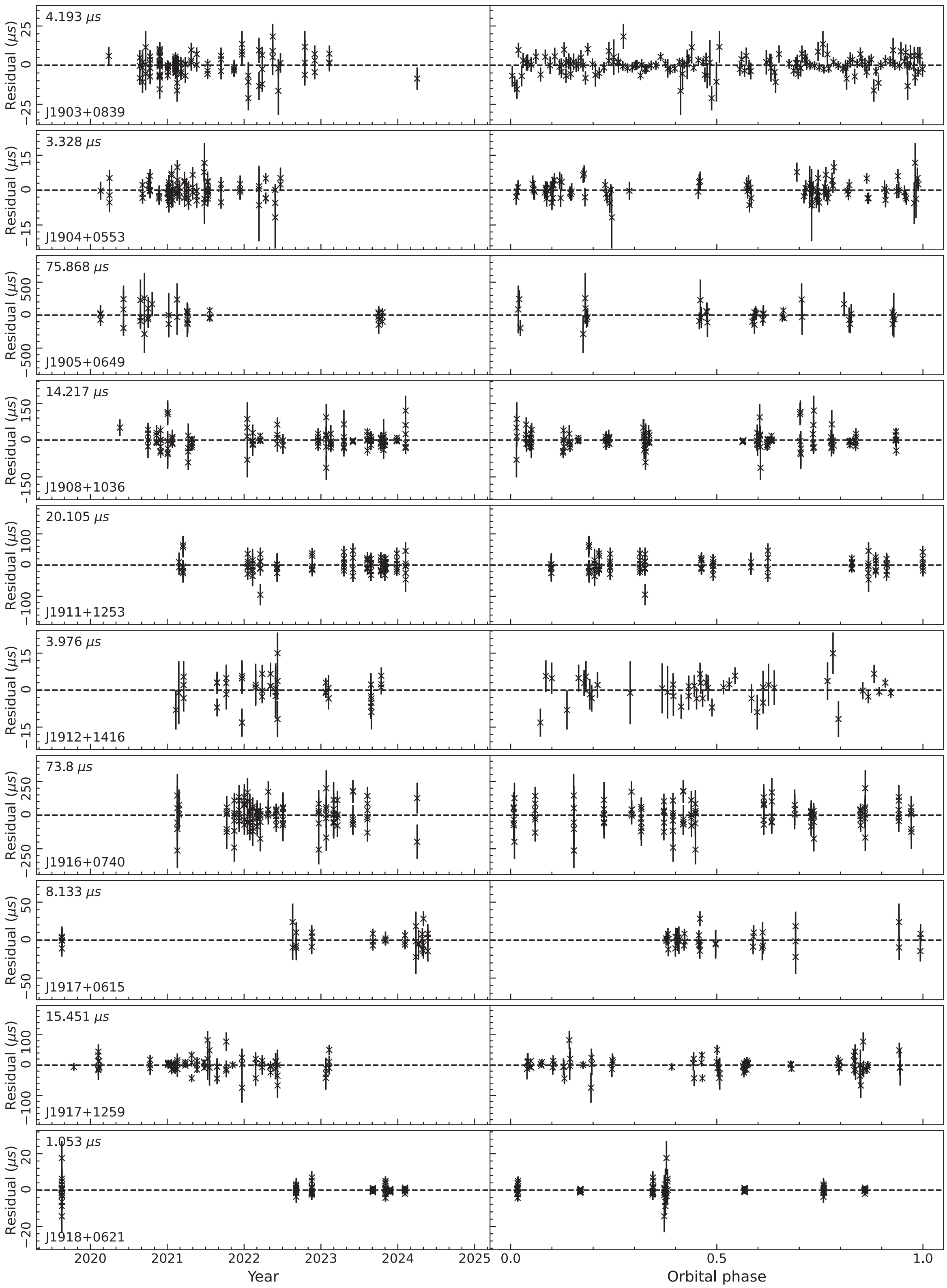

Figure A1. (Continued.)

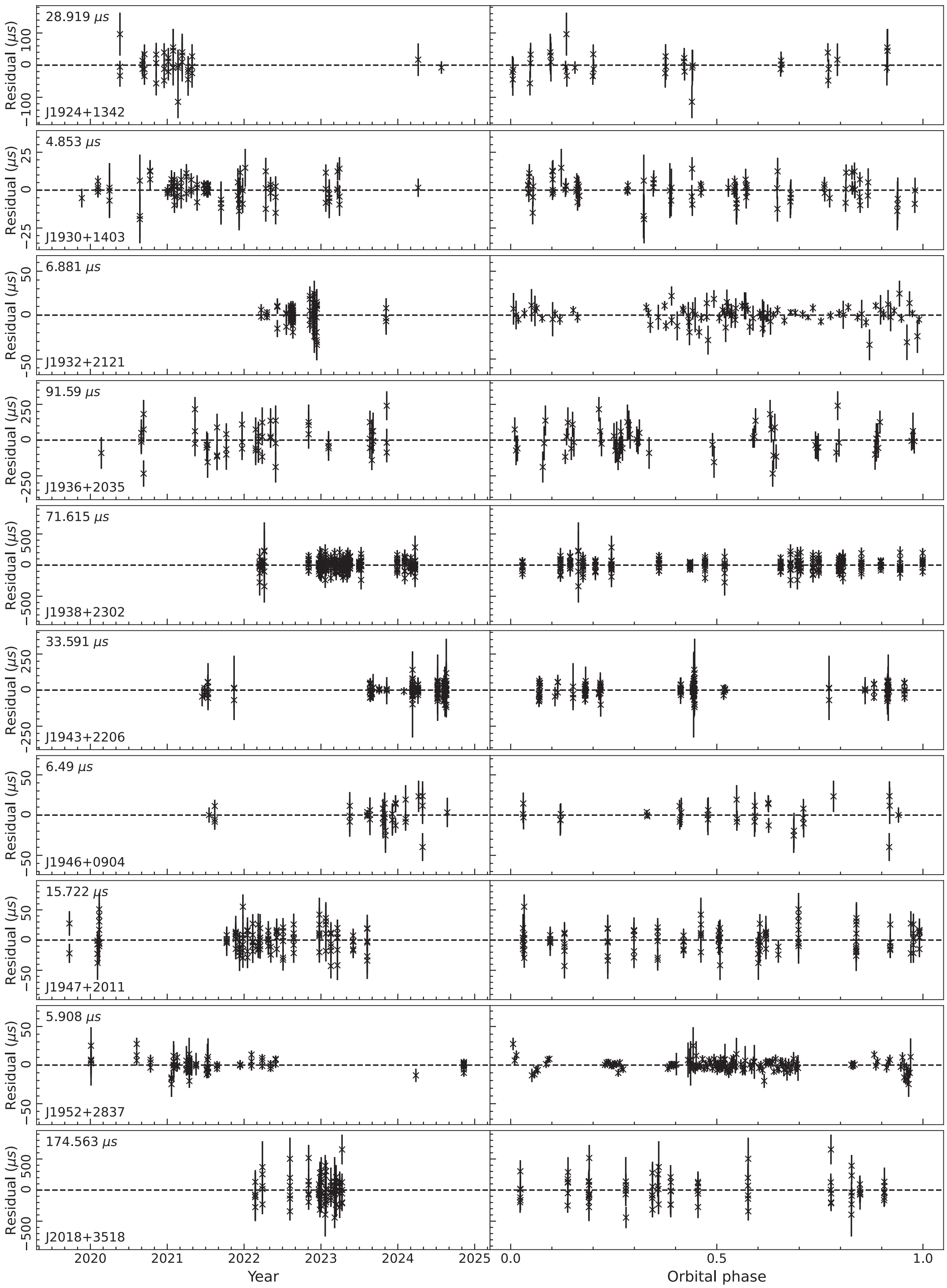

Figure A1. (Continued.)

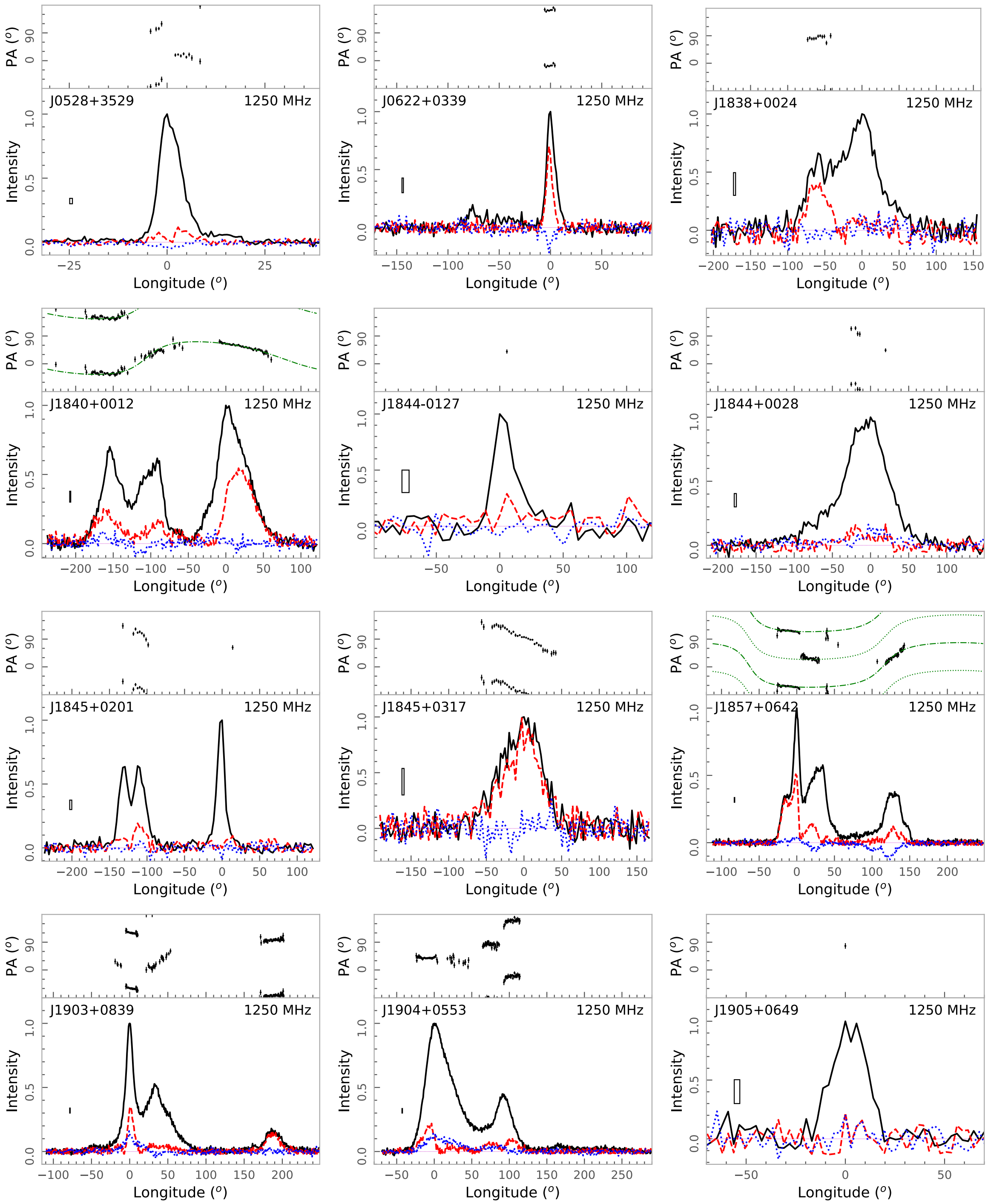

Figure A2. Integrated pulse profiles of 29 pulsars. The total intensity, linear and circular polarization are represented by solid, dashed and dotted lines in the bottom sub-panel. The left-hand circular polarization is defined to be positive. The bin size and 3σ are marked inside the sub-panel, here σ is the standard deviation of off-pulse bins. In the top panel, dots with error bars are measurements of polarization position angles for linear polarization intensity exceeding 3σ line. The position angles are corrected to infinite frequency by discounting Faraday rotation. We tried to fit the polarization angle curves with the rotating vector model (Radhakrishnan & Cooke 1969) for 5 pulsars, PSRs J1840+0012, J1857+0642, J1916+0740, J1930+1403 and J1946+0904.

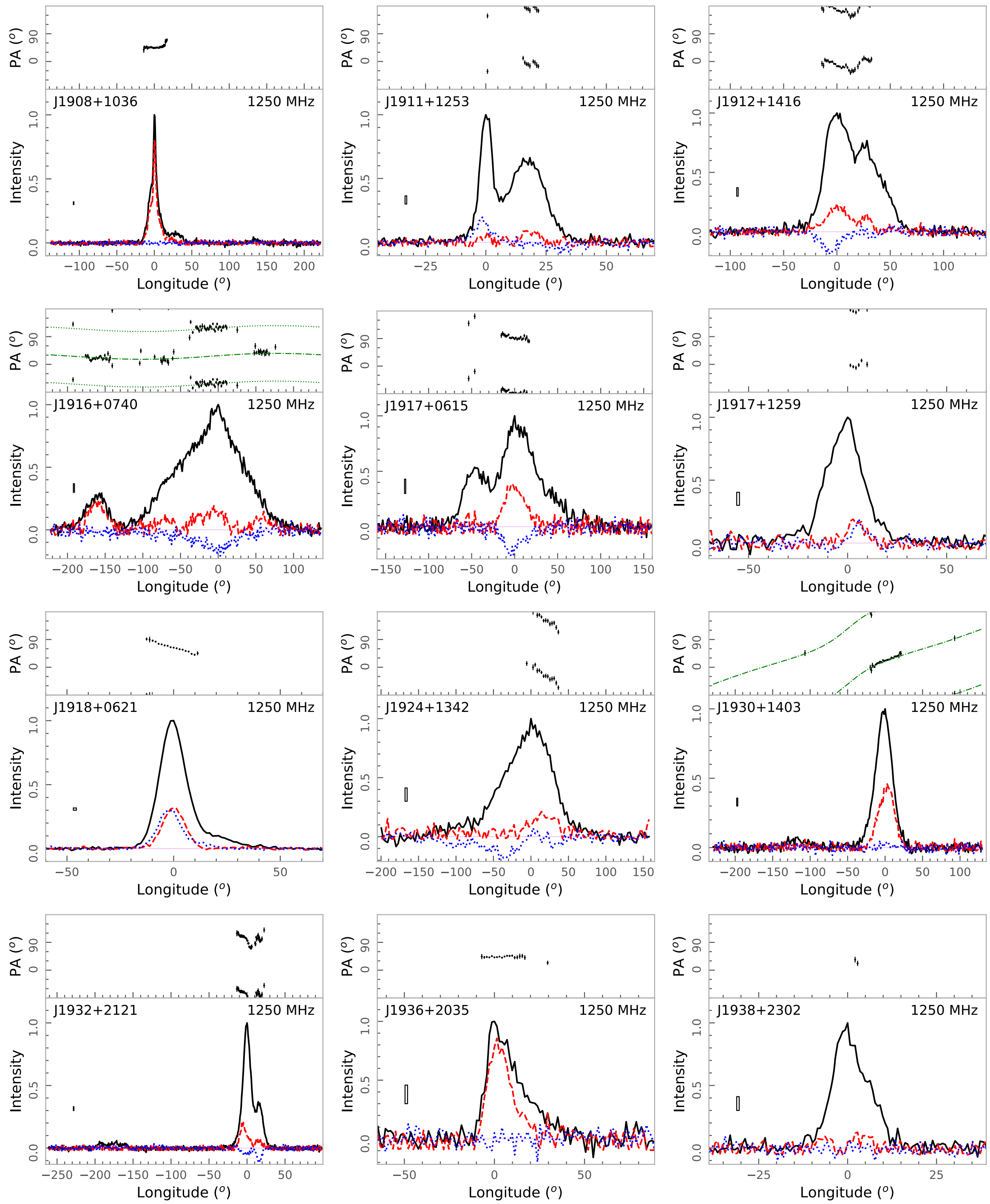

Figure A2. (Continued.)

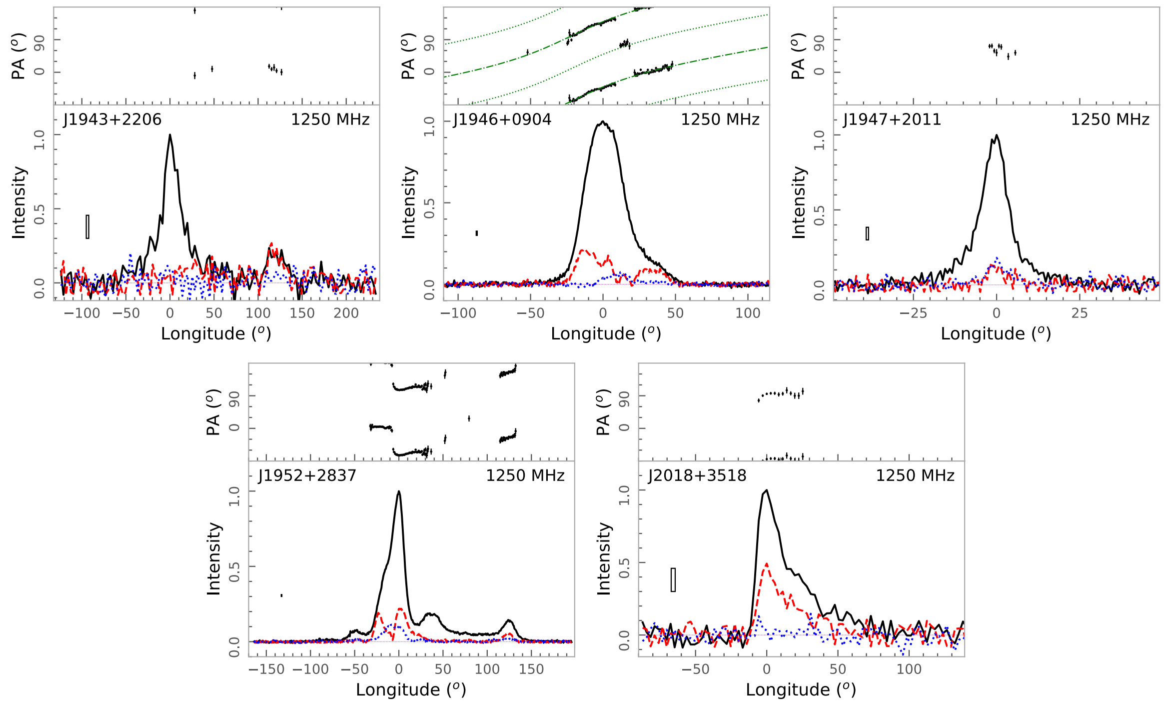

Figure A2. (Continued.)

model, the Barycentric Dynamical Time (TDB) units, and the TT(TAI) clock. The ephemeris items include the standard pulsar name defined by accurate position, the temperate name and the GPPS discovery number, the MJD range and the span for FAST observation data and the number of TOAs. Measured quantities include: R.A. in hh:mm:ss.ss, Decl. in ±dd:mm:ss.s, DM in cm^{-3} pc, pulsar rotation frequency ν in Hz, the first derivative of pulsar rotation frequency $\dot{\nu}$ in 10^{-16} Hz s^{-1}, proper motion in R.A. $\mu_\alpha \cos\delta$ in milli-arc-second (mas) per year (if measured), proper motion in Decl. μ_δ is in milli-arc-second (mas) per year (if measured), the timing residual in microsecond (μs); timing residual scaling factor EFAC; timing residual quadratic adding factor EQUAD; Reduced χ^2 of model-fitting. Binary parameters include orbital period P_b in days, projected semimajor axis of pulsar's orbit x in light-seconds, the time of passing through periastron T_0 (if measured), the longitude of periastron ω (if measured), time of ascending node T_{asc} in MJD, first and second Laplace parameters e_1 and e_2. (3) Derived quantities include: the Galactic longitude l in degree, the Galactic latitude b in degree, distance estimates D_{YMW} and D_{NE2001} by using the Galactic electron density distribution models YMW17 (Yao et al. 2017) and NE2001 (Cordes & Lazio 2002) in kpc, the spin period of a pulsar P in millisecond, the derivative of the spin period $\dot{P}$ in second per second, characteristic age τ in Gyr, surface magnetic field strength B_{surf} in 10^8 G, and the orbital eccentricity e (if measured).

Timing residuals of 29 binary pulsars are shown in Figure A1. The left panels are for the residuals along the observation epochs, and the right panels are for residuals versus the orbital phase.

For these pulsars with timing solution, we can add all FAST polarization measurements and get their polarization profiles, as shown in Figure A2. We tried to fit the polarization angle curves with the rotating vector model (Radhakrishnan & Cooke 1969) for 5 pulsars, PSRs J1840+0012, J1857+0642, J1916+0740, J1930+1403 and J1946+0904.

For 78 binary pulsars without timing solutions, the measurements of barycentric periods are plotted across the orbit phase in Figure A3, together with the currently best-fitting

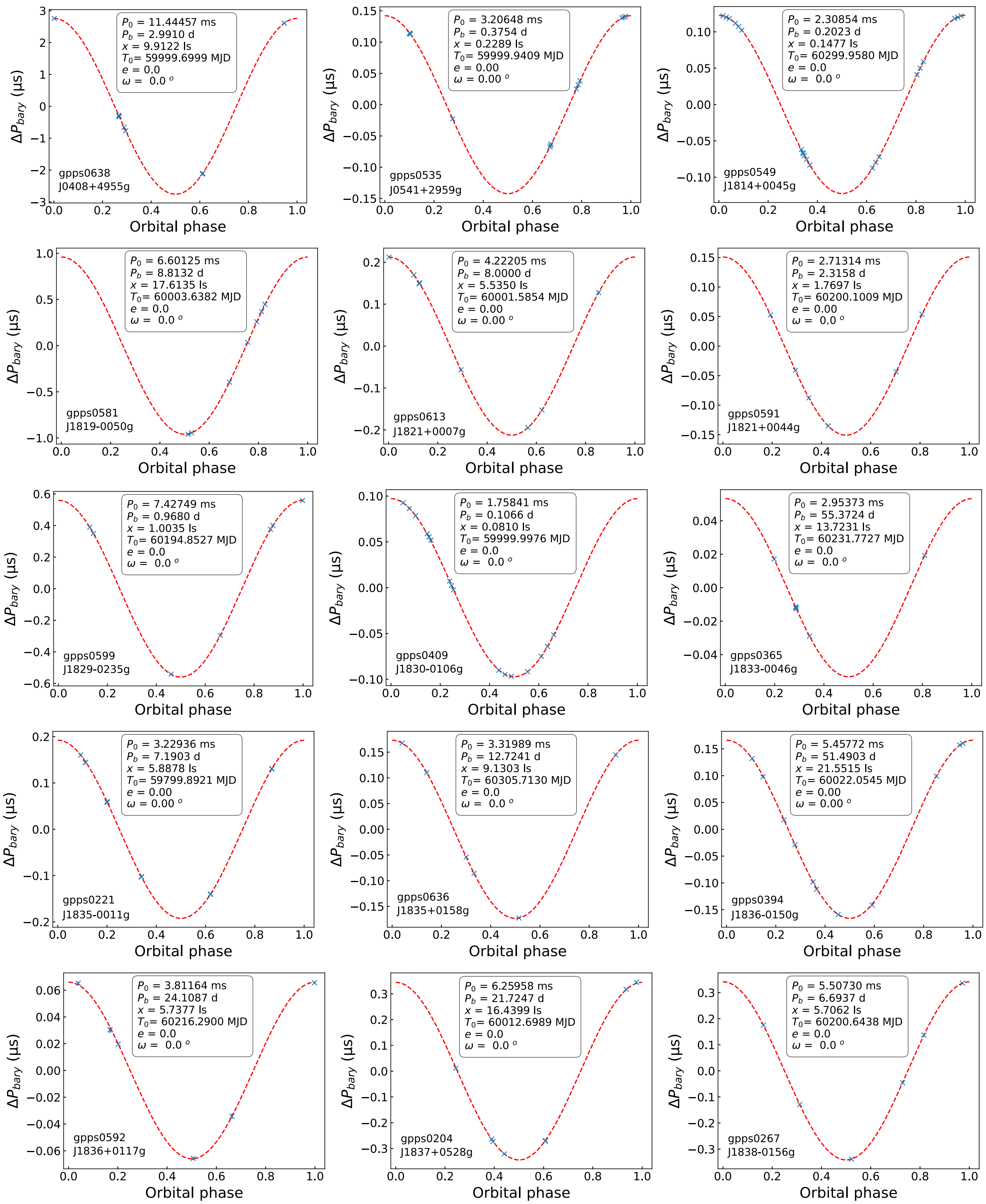

Figure A3. Variations of barycentric periods for 78 binary pulsars across the orbit phase. For each pulsar, the observed barycentric periods are marked by "x" after the average period P_0 is subtracted. The error bars are marked but too small to see for most data. The dashed line is the best-fit by using the preliminary Keplerian model with orbital parameters (P_b, x, T_0, e and ω) listed inside the panel. The orbital phase is referred to as the periastron of the orbit.

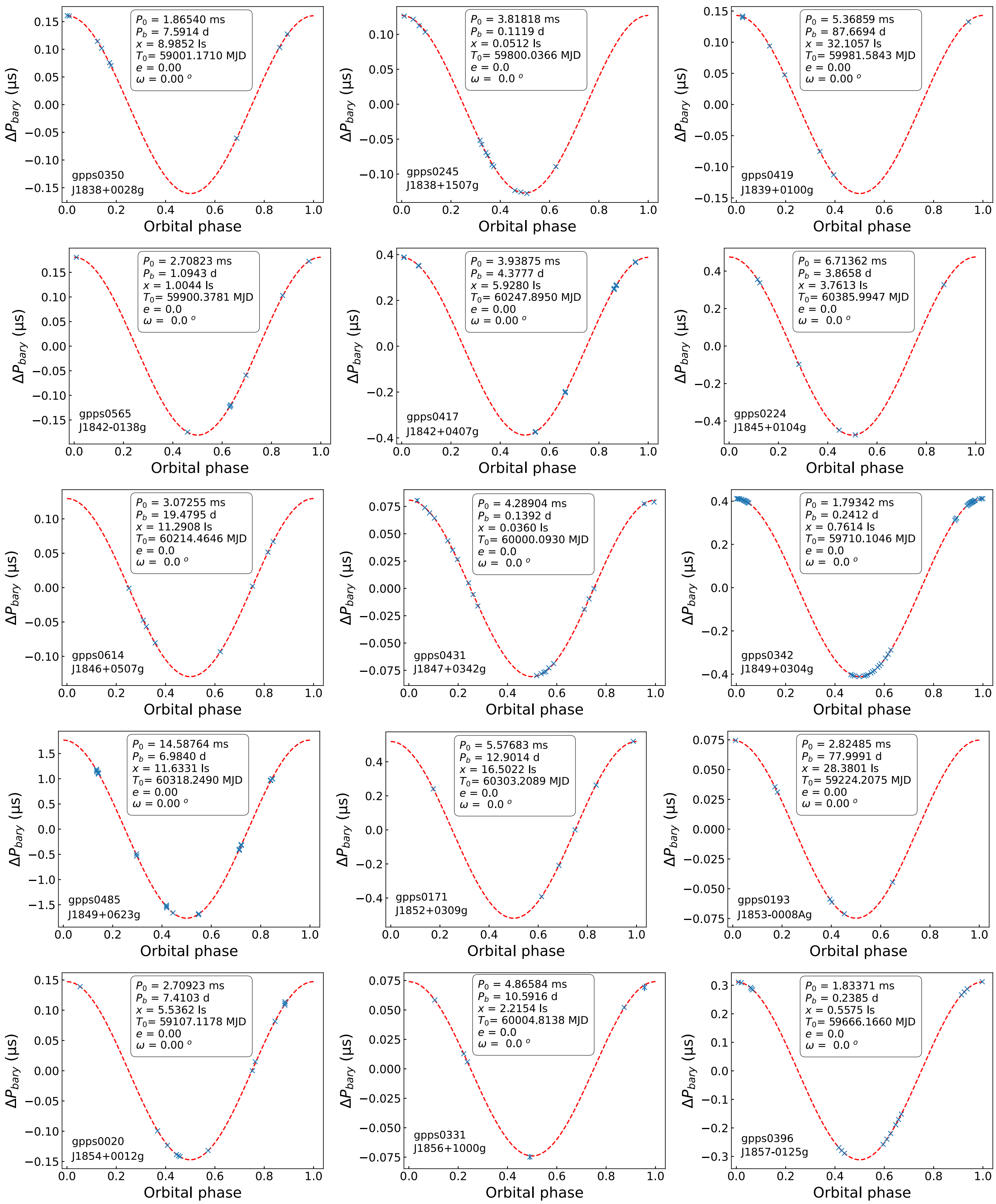

Figure A3. (Continued.)

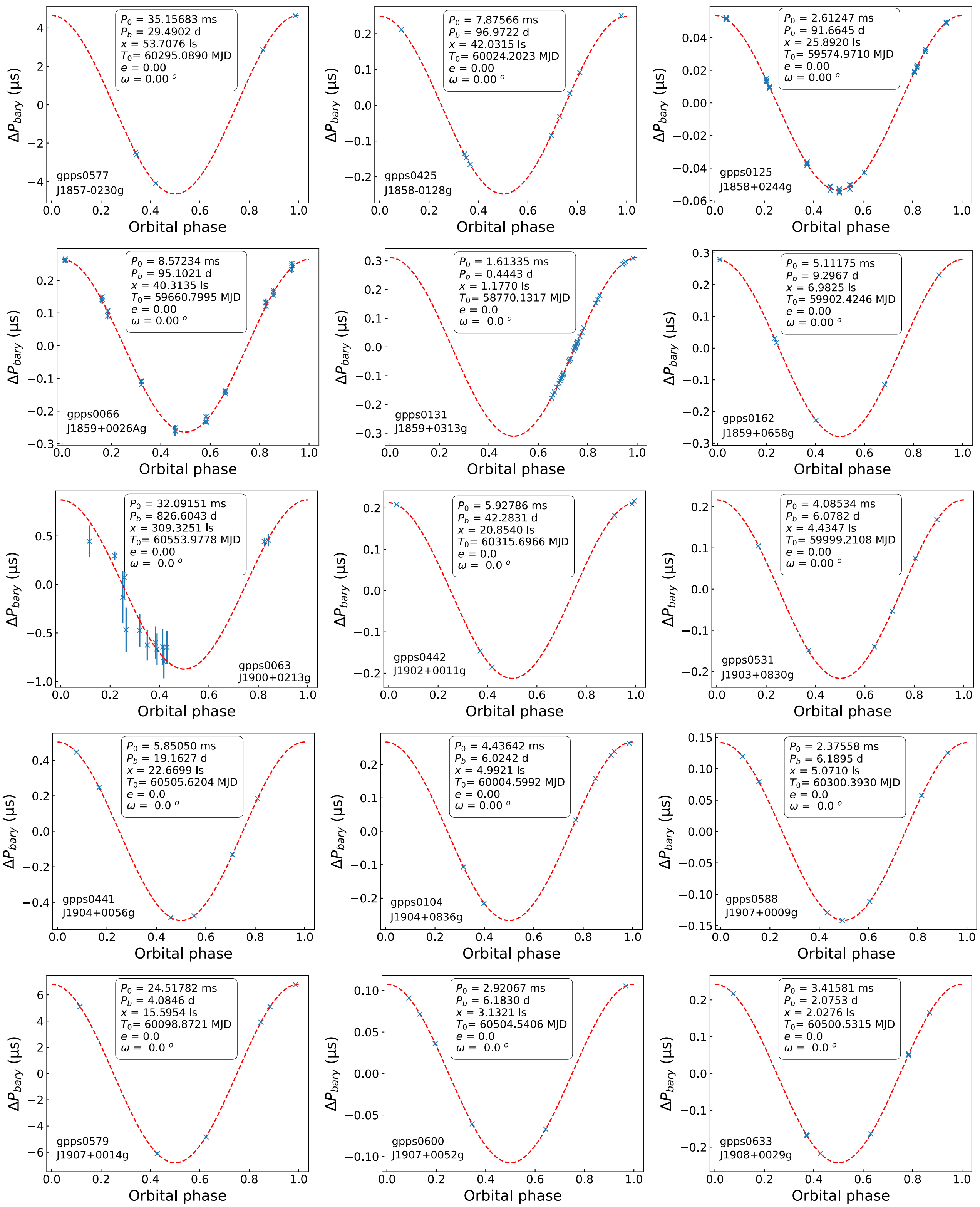

Figure A3. (Continued.)

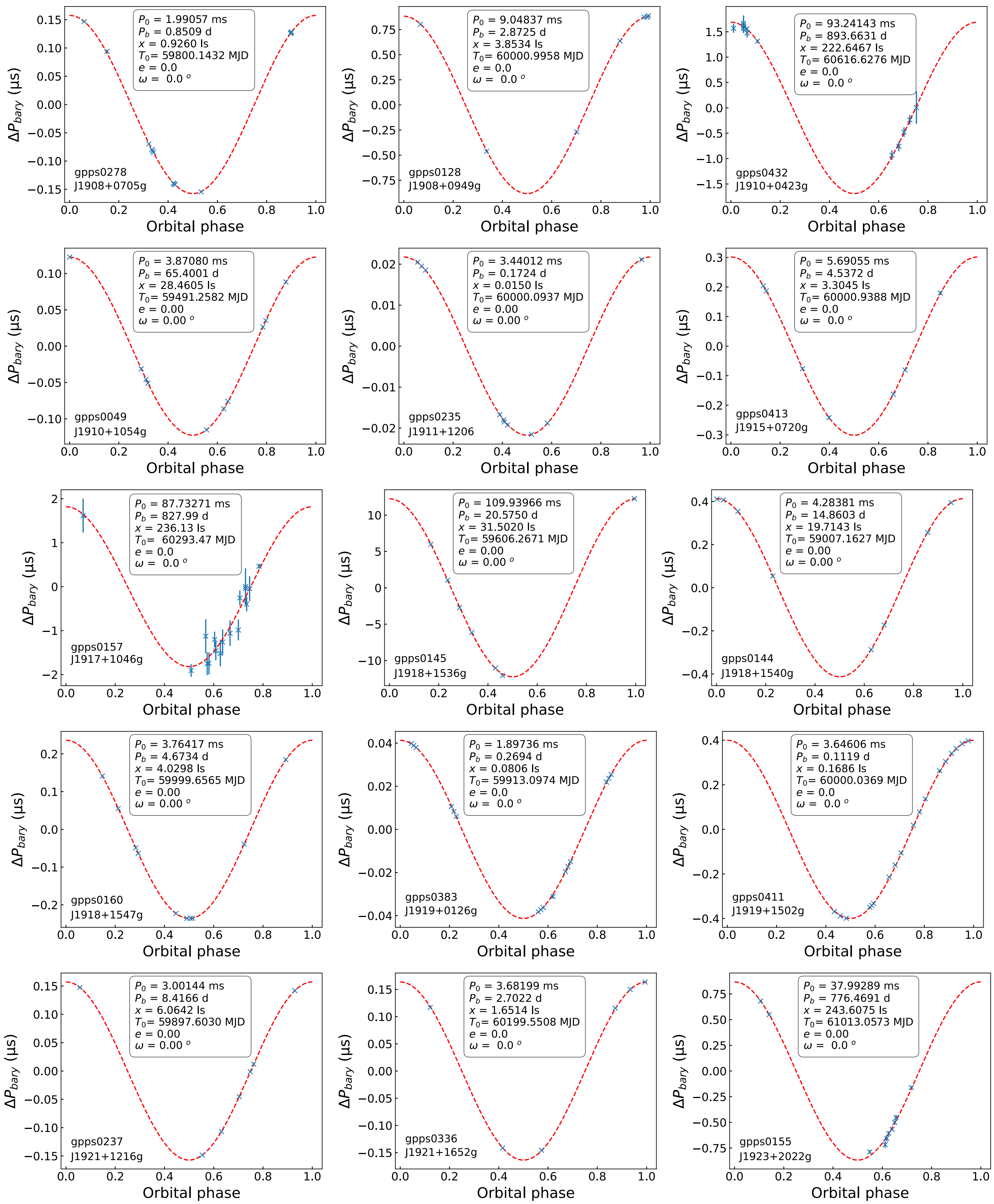

Figure A3. (Continued.)

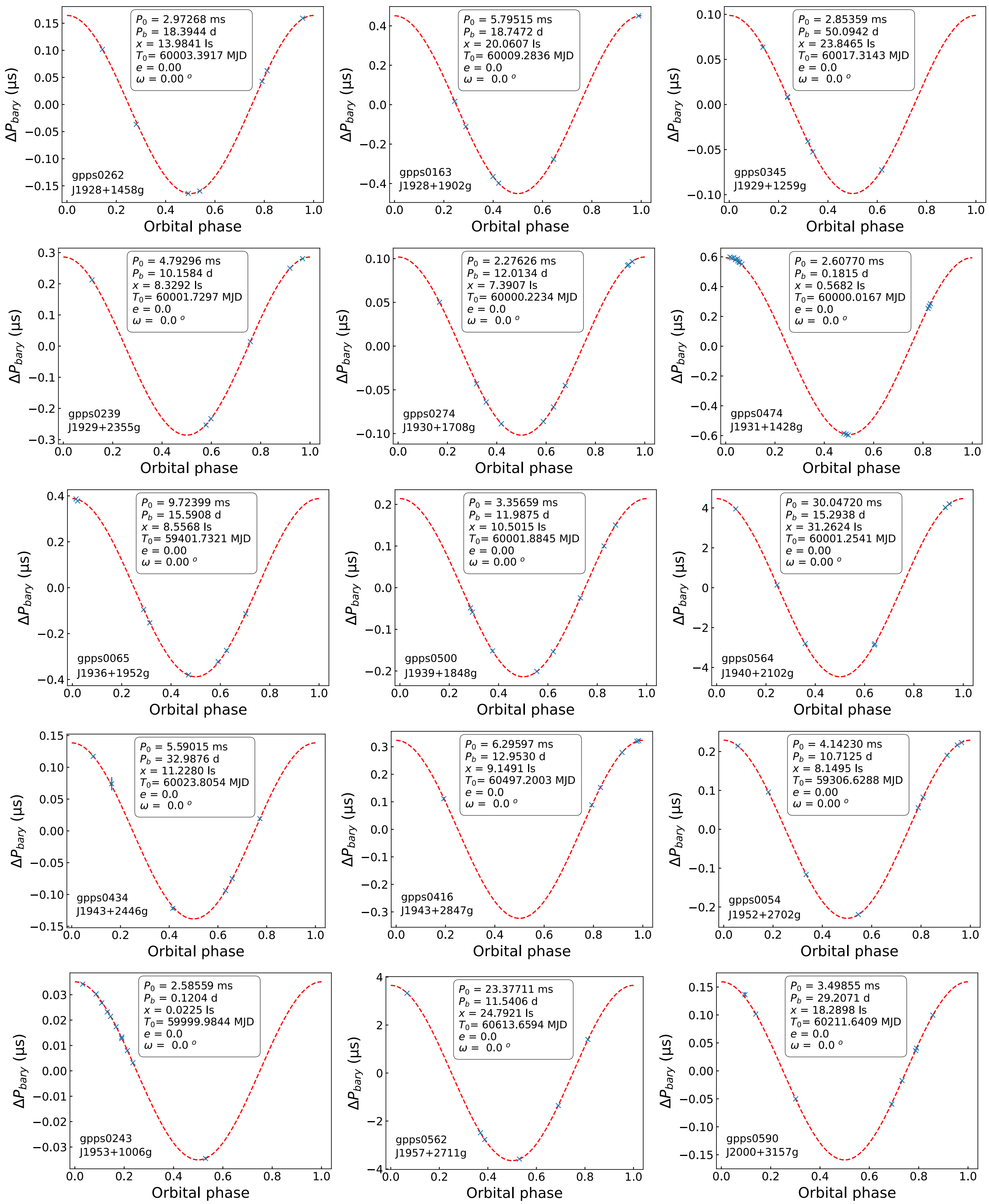

Figure A3. (Continued.)

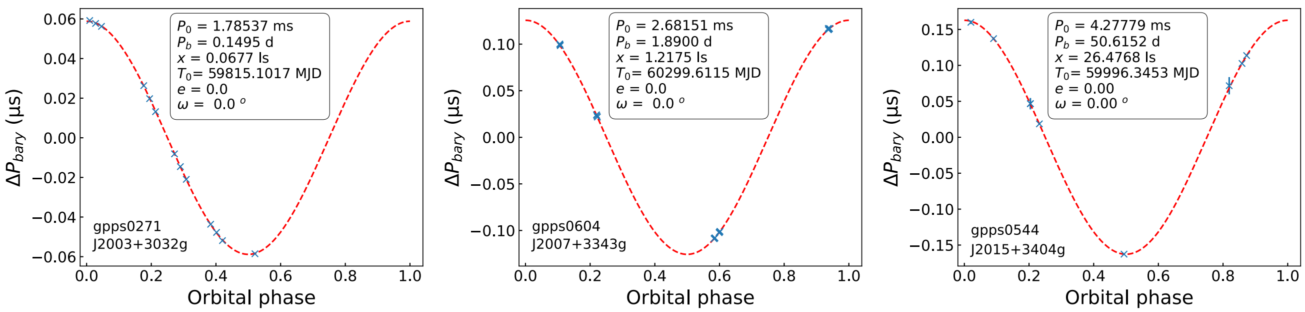

Figure A3. (Continued.)

preliminary Keplerian model. These data are the base for further follow-up observations.

ORCID iDs

P. F. Wang https://orcid.org/0000-0002-6437-0487
J. L. Han https://orcid.org/0000-0002-9274-3092
Z. L. Yang https://orcid.org/0009-0009-6590-1540
T. Wang https://orcid.org/0000-0002-4704-5340
C. Wang https://orcid.org/0009-0004-3433-2027
W. Q. Su https://orcid.org/0009-0003-2212-4792
J. Xu https://orcid.org/0000-0003-1778-5580
D. J. Zhou https://orcid.org/0000-0002-6423-6106
Yi Yan https://orcid.org/0009-0008-1612-9948
W. C. Jing https://orcid.org/0000-0002-1056-5895
N. N. Cai https://orcid.org/0000-0002-5915-5539

References

Alam, M. F., Arzoumanian, Z., Baker, P. T., et al. 2021, ApJS, 252, 5
Alpar, M. A., Cheng, A. F., Ruderman, M. A., & Shaham, J. 1982, Natur, 300, 728
Antoniadis, J. 2014, ApJL, 797, L24
Antoniadis, J., Freire, P. C. C., Wex, N., et al. 2013, Sci, 340, 448
Antoniadis, J., Tauris, T. M., Ozel, F., et al. 2016, arXiv:1605.01665
Backer, D. C., & Hellings, R. W. 1986, ARA&A, 24, 537
Bhattacharya, D., & van den Heuvel, E. P. J. 1991, PhR, 203, 1
Blandford, R., & Teukolsky, S. A. 1976, ApJ, 205, 580
Cameron, A. D., Champion, D. J., Kramer, M., et al. 2018, MNRAS, 475, L57
Chambers, K. C., Magnier, E. A., Metcalfe, N., et al. 2016, arXiv:1612.05560
Chen, H.-L., Chen, X., Tauris, T. M., & Han, Z. 2013, ApJ, 775, 27
Chen, H.-L., Tauris, T. M., Han, Z., & Chen, X. 2021, MNRAS, 503, 3540
Corbet, R. H. D. 1984, A&A, 141, 91
Cordes, J. M., & Lazio, T. J. W. 2002, arXiv:astro-ph/0207156
Damour, T., & Deruelle, N. 1985, AIHPA, 43, 107
Demorest, P. B., Pennucci, T., Ransom, S. M., Roberts, M. S. E., & Hessels, J. W. T. 2010, Natur, 467, 1081
Deneva, J. S., Ray, P. S., Camilo, F., et al. 2021, ApJ, 909, 6
Du, Z.-X., Yu, Y.-W., Chen, A. M., et al. 2023, RAA, 23, 125024
Freire, P. C., Kramer, M., & Lyne, A. G. 2001, MNRAS, 322, 885
Freire, P. C. C., Bassa, C. G., Wex, N., et al. 2011, MNRAS, 412, 2763
Freire, P. C. C., & Ridolfi, A. 2018, MNRAS, 476, 4794
Freire, P. C. C., Wex, N., Esposito-Farèse, G., et al. 2012, MNRAS, 423, 3328
Guo, Y., Wang, B., & Li, X. 2024, MNRAS, 527, 7394
Han, J. L., Wang, C., Wang, P. F., et al. 2021, RAA, 21, 107
Han, J. L., Zhou, D. J., Wang, C., et al. 2025, RAA, 25, 014001
Hobbs, G., Guo, L., Caballero, R. N., et al. 2020, MNRAS, 491, 5951
Hobbs, G. B., Edwards, R. T., & Manchester, R. N. 2006, MNRAS, 369, 655
Hotan, A. W., van Straten, W., & Manchester, R. N. 2004, PASA, 21, 302
Hu, H., Kramer, M., Wex, N., Champion, D. J., & Kehl, M. S. 2020, MNRAS, 497, 3118
Hui, C. Y., Wu, K., Han, Q., Kong, A. K. H., & Tam, P. H. T. 2018, ApJ, 864, 30
Istrate, A. G., Tauris, T. M., & Langer, N. 2014, A&A, 571, A45
Ivanova, N., Justham, S., Chen, X., et al. 2013, A&ARv, 21, 59
Jiang, P., Tang, N.-Y., Hou, L.-G., et al. 2020, RAA, 20, 064
Kaspi, V. M., Lyne, A. G., Manchester, R. N., et al. 2000, ApJ, 543, 321
Koester, D., & Reimers, D. 2000, A&A, 364, L66
Kramer, M., Stairs, I. H., Manchester, R. N., et al. 2006, Sci, 314, 97
Kramer, M., Stairs, I. H., Venkatraman Krishnan, V., et al. 2021, MNRAS, 504, 2094
Lange, C., Camilo, F., Wex, N., et al. 2001, MNRAS, 326, 274
Lentati, L., Taylor, S. R., Mingarelli, C. M. F., et al. 2015, MNRAS, 453, 2576
Li, D., Lin, F. X., Main, R., et al. 2019, MNRAS, 484, 5723
Main, R., Yang, I. S., Chan, V., et al. 2018, Natur, 557, 522
Manchester, R. N., Hobbs, G. B., Teoh, A., & Hobbs, M. 2005, AJ, 129, 1993
Miao, C. C., Zhu, W. W., Li, D., et al. 2023, MNRAS, 518, 1672
Nan, R. 2006, ScChG, 49, 129
Nan, R., Li, D., Jin, C., et al. 2011, IJMPD, 20, 989
Nice, D. J., & Taylor, J. H. 1995, ApJ, 441, 429
Özel, F., & Freire, P. 2016, ARA&A, 54, 401
Pan, Z., Lu, J. G., Jiang, P., et al. 2023, Natur, 620, 961
Park, R. S., Folkner, W. M., Williams, J. G., & Boggs, D. H. 2021, AJ, 161, 105
Phinney, E. S. 1992, RSPTA, 341, 39
Phinney, E. S., & Kulkarni, S. R. 1994, ARA&A, 32, 591
Podsiadlowski, P. 1991, Natur, 350, 136
Podsiadlowski, P., Rappaport, S., & Pfahl, E. D. 2002, ApJ, 565, 1107
Pylyser, E., & Savonije, G. J. 1988, A&A, 191, 57
Radhakrishnan, V., & Cooke, D. J. 1969, ApL, 3, 225
Reardon, D. J., Shannon, R. M., Cameron, A. D., et al. 2021, MNRAS, 507, 2137
Refsdal, S., & Weigert, A. 1971, A&A, 13, 367
Roberts, M. S. E. 2013, in IAU Symp. 291, Neutron Stars and Pulsars: Challenges and Opportunities after 80 years, ed. J. van Leeuwen (Cambridge: Cambridge Univ. Press), 127
Strader, J., Chomiuk, L., Cheung, C. C., et al. 2015, ApJL, 804, L12
Strader, J., Swihart, S., Chomiuk, L., et al. 2019, ApJ, 872, 42
Su, W. Q., Han, J. L., Yang, Z. L., et al. 2024, MNRAS, 530, 1506
Taam, R. E., King, A. R., & Ritter, H. 2000, ApJ, 541, 329
Tauris, T. M. 1996, A&A, 315, 453

Tauris, T. M. 2011, in ASP Conf. Ser. 447, Evolution of Compact Binaries, ed. L. Schmidtobreick, M. R. Schreiber, & C. Tappert (San Francisco, CA: ASP), 285
Tauris, T. M., Kramer, M., Freire, P. C. C., et al. 2017, ApJ, 846, 170
Tauris, T. M., Langer, N., & Kramer, M. 2011, MNRAS, 416, 2130
Tauris, T. M., Langer, N., & Kramer, M. 2012, MNRAS, 425, 1601
Tauris, T. M., & Savonije, G. J. 1999, A&A, 350, 928
Tauris, T. M., & van den Heuvel, E. P. J. 2006, Compact Stellar X-ray Sources, Vol. 39 (Cambridge: Cambridge Univ. Press), 623
Tauris, T. M., & van den Heuvel, E. P. J. 2023, Physics of Binary Star Evolution. From Stars to X-ray Binaries and Gravitational Wave Sources (Princeton, NJ: Princeton Univ. Press)
van Haaften, L. M., Nelemans, G., Voss, R., Wood, M. A., & Kuijpers, J. 2012, A&A, 537, A104
van Straten, W., & Bailes, M. 2011, PASA, 28, 1
Venkatraman Krishnan, V., Bailes, M., van Straten, W., et al. 2020, Sci, 367, 577
Voisin, G., Cognard, I., Freire, P. C. C., et al. 2020, A&A, 638, A24
Wang, P. F., Han, J. L., Xu, J., et al. 2023, RAA, 23, 104002
Webbink, R. F., Rappaport, S., & Savonije, G. J. 1983, ApJ, 270, 678
Weisberg, J. M., & Huang, Y. 2016, ApJ, 829, 55
Weisberg, J. M., & Taylor, J. H. 1984, PhRvL, 52, 1348
Xu, H., Chen, S., Guo, Y., et al. 2023, RAA, 23, 075024
Yang, Z. L., Han, J. L., Jing, W. C., & Su, W. Q. 2023, ApJL, 956, L39
Yang, Z. L., Han, J. L., Wang, T., et al. 2025a, RAA, 25, 014002
Yang, Z. L., Han, J. L., Zhou, D. J., et al. 2025b, Sci, submitted
Yao, J. M., Manchester, R. N., & Wang, N. 2017, ApJ, 835, 29